

Glacial abrupt climate change as a multi-scale phenomenon resulting from monostable excitable dynamics

Keno Riechers
Complexity Science
Potsdam Institute for Climate Impact Research
Potsdam, Germany
riechers@pik-potsdam.de

Georg Gottwald
School of Mathematics and Statistics
University of Sydney
Sydney, Australia

Niklas Boers
Earth System Modelling - School of Engineering & Design
Technical University of Munich
Munich, Germany

May 23, 2023

Paleoclimate proxy records evidence repeated abrupt climatic transitions during past glacial intervals with strongest expression in the North Atlantic region. In particular, temperature reconstructions from Greenland ice cores reveal high northern latitude warming events of up to 16°C on decadal time scales, but associated impacts extend across the globe. These so-called Dansgaard-Oeschger (DO) events are followed by phases of relatively mild temperatures termed interstadials, which exhibit gradual cooling over several hundred to a few thousand years prior to a final phase of abrupt temperature decrease back to cold stadials. To date, there is no consensus on the mechanism of this millennial-scale variability. Here, we propose an excitable model system to explain the DO cycles, in which interstadials occur as noise-induced state space excursions. Our model comprises the mutual multi-scale interactions between four dynamical variables representing Arctic atmospheric temperatures, Nordic Seas' temperatures and sea ice cover, and the Atlantic Meridional Overturning Circulation (AMOC). Crucially, the model's atmosphere-ocean heat flux is moderated by the sea ice variable, which in turn is subject to large perturbations dynamically generated by fast evolving intermittent noise. If supercritical, these perturbations trigger interstadial-like state space excursions seizing all four model variables. As a physical source for such a driving noise process we propose convective events in the ocean or atmospheric blocking events. The key characteristics of DO cycles are reproduced by our model with remarkable resemblance to the proxy record; in particular, their shape, return time, as well as the dependence of the interstadial and stadial durations on the background temperatures are reproduced accurately. In contrast to the prevailing understanding that the DO variability showcases bistability in the underlying dynamics, we conclude that multi-scale, monostable excitable dynamics provides a promising alternative candidate to explain the millennial-scale climate variability associated with the DO events.

Keywords Dansgaard-Oeschger Events | Excitable Dynamics | Multi-scale System | α -stable Noise

1 Introduction

Stable water isotope records from Greenland ice cores provide evidence for repeated abrupt climatic shifts during the last glacial interval. Decadal-scale transitions from low to high values of $\delta^{18}\text{O}$ (Fig. 1a) are indicative of sudden warming events at the drilling site, which are termed Dansgaard-Oeschger (DO) events [1–5]. The temperature increases of $\sim 8 - 16^{\circ}\text{C}$ [6–10] are followed by phases of milder, yet moderately cooling temperatures called interstadials, lasting from centuries to millennia [11–13]. Typically, a final and more abrupt decline brings the climate back to a colder state known as stadial climate. The successions of interstadials and stadials are often

referred to as DO cycles.

While the early glacial ($\sim 115\text{--}71$ kyr b2k) was dominated by long lasting interstadials and relatively warm stadial conditions, colder stadials and very short interstadials prevailed during the later part of the last glacial ($\sim 29\text{--}14$ kyr b2k, compare Fig. 1). The middle part ($\sim 71\text{--}29$ kyr b2k) was characterized by frequent DO events with intermediate-length stadials and interstadials. The ratio between interstadial and stadial duration was presumably influenced by the background climate state and orbital forcing [14–18].

The signature of DO cycles is found in numerous paleoclimatic proxy records around the globe, including speleothems and Antarctic ice cores [25, 26]. For instance, DO events

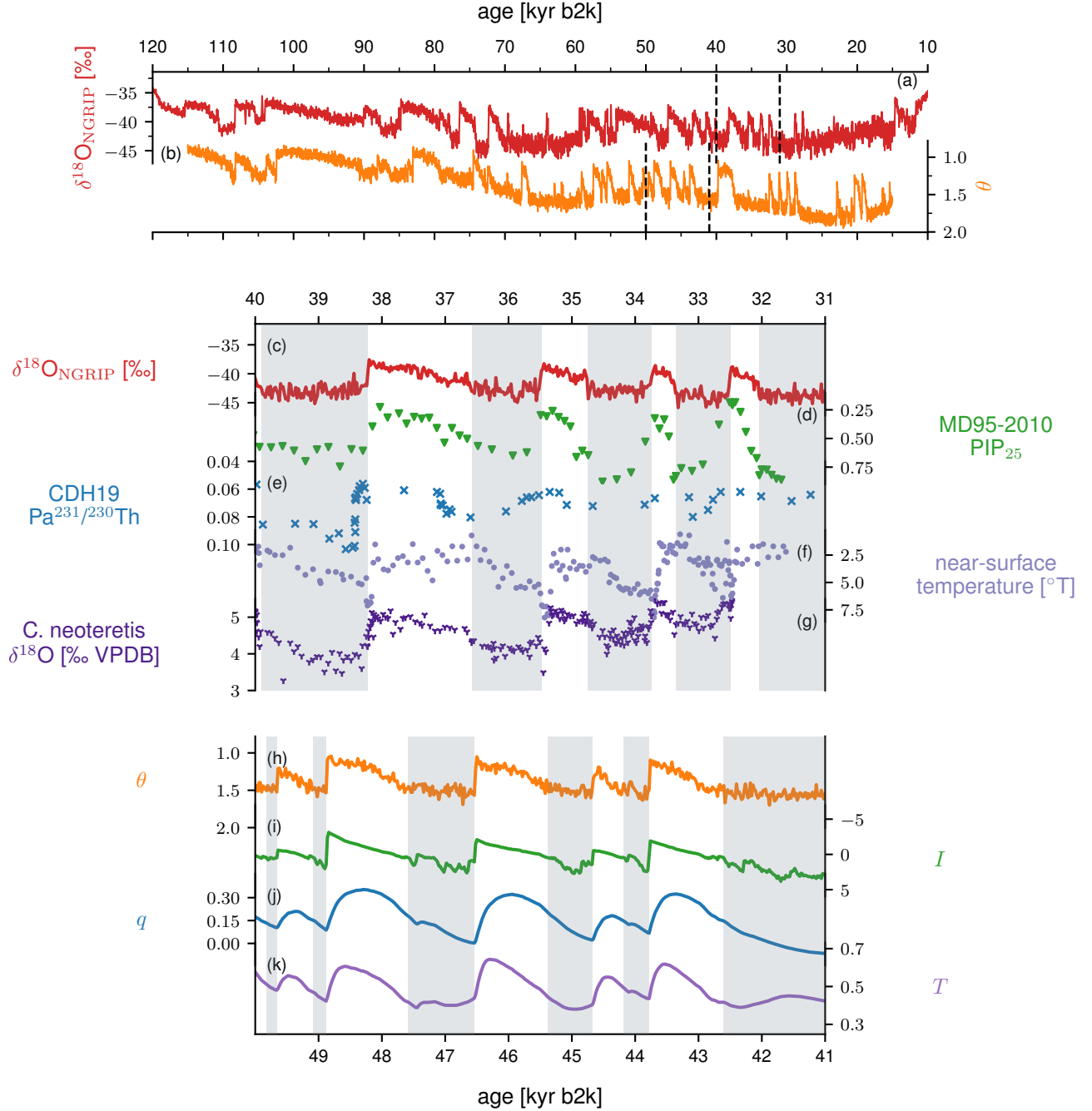


Figure 1: Paleoclimatic proxy evidence for characteristic features of DO variability together with corresponding results of our model defined by Eqs. 1–7. (a) 20-year mean NGRIP $\delta^{18}\text{O}$ data [12, 19] interpreted as a qualitative proxy of air temperatures over Greenland (data available at: <https://www.iceandclimate.nbi.ku.dk/data/>, last access: 3 March 2023). (b) Simulated Arctic atmospheric air temperatures θ . (c) Zoom into the period 40–31 kyr b2k of (a) — the period was chosen due to the availability of proxy data. (d) PIP₂₅ index from the marine sediment core MD95-2010 [20]. The PIP₂₅ index is indicative of past sea ice cover at the core site with values of 1 and 0 corresponding to perennial sea ice and open ocean conditions, respectively. (e) Pa/Th ratios from the marine sediment core CDH19 from the Bermuda Rise as provided by [21]. The ratios are interpreted as a direct measure of the AMOC strength, with lower values corresponding to stronger overturning and vice versa. (f) Near-surface ocean temperature reconstruction from the marine sediment core MD99-2284 [22], presented here on a revised age scale [20, 23]. (g) $\delta^{18}\text{O}$ of the benthic species *C. neoteretis* [22] shown on a revised age-scale [20, 23]. According to the most recent interpretation of the data, the benthic $\delta^{18}\text{O}$ is mostly indicative of past deep-ocean temperatures [20, 24] with higher values indicating colder temperatures and vice versa. Panels (h)–(k) show corresponding model results but for the period 50–41 kyr b2k, which was selected because of its high DO event frequency. (h) the Arctic atmospheric temperature θ , (i) the Nordic Seas' sea ice cover I , (j) the AMOC strength q and (k) the Nordic Seas intermediate to deep water temperatures T . The proxy records shown in (c)–(g) should be directly compared to the simulated trajectories shown in panels (h)–(k), respectively. All model variables are given in arbitrary units.

are associated with large-scale reorganizations of the Northern Hemisphere atmospheric circulation [27–29] including a northward shift of the ITCZ [26] with strong impacts on the Asian and South American Monsoon systems [30–34]. The expression of DO variability is, however, most pronounced in the North Atlantic region and climatic processes hosted by this region such as sea ice or deep water formation are believed to be central to the triggering mechanism of DO events.

To date there is no conclusive theory that fully explains the mechanism of the DO cycles. Several climatic components have been proposed to be relevant, including ocean dynamics, atmospheric events, sea ice, ice sheets and freshwater fluxes [18, 22, 35–40]. Similarly, several dynamic mechanisms have been invoked to explain the DO events, ranging from external drivers such as (periodically) changing freshwater fluxes [36, 41–43] and noise induced transitions between two stable states [17, 44–47] to dynamically self-generating mechanisms including self-sustained oscillations [18, 22, 35, 39, 48–50]. In this study, building on the results of [51] we consider a paradigm for DO variability which has to date received only little attention: We present an excitable multi-scale model, whose single stable fixed point can be identified with stadial climate conditions. In response to perturbations above a critical threshold, the system takes prolonged excursions through a region of slow transitive dynamics in state space assuming an interstadial configuration in all system dimensions. The perturbations are generated by an intermittent non-Gaussian driving noise detailed later. In particular, we reproduce the following five central aspects of DO cycles in an interpretable manner:

1. **Shape of DO cycles:** In addition to the above described characteristic evolution of past Greenland atmospheric temperatures over a DO cycle we resolve more detailed features of the record, such as the presence of short-lived interstadials and stadials (cf. Fig. 1a and c).
2. **Duration of stadials and interstadials:** A pronounced variability in stadial and interstadial duration can be observed over the last glacial (cf. Fig. 1a). It has previously been shown that the interstadial durations are positively correlated with slowly varying global mean background climate [18], while the variability in stadial durations is less clear.
3. **In-phase sea ice dynamics:** An important climate variable found to vary in phase with Greenland temperatures is the sea ice extent in the Nordic Seas and the North Atlantic. During stadials an extensive sea ice cover prevails, whereas interstadials exhibit conditions ranging from open water to seasonal sea ice cover [20, 22, 52–54] (cf. Fig. 1d).
4. **Nordic Seas’ temperature inversion:** Several studies report warming of the ice-covered stadial Nordic Seas at intermediate and large depth which they attribute to continued inflow of warm water masses from the south [22, 24, 49] (cf. Fig. 1f and g). This heat — initially trapped under the sea ice — is hypothesized to have warmed the polar atmosphere abruptly in response to sudden sea ice retreat during DO events [18, 22].

5. **AMOC switches:** Multiple lines of direct and indirect evidence, thoroughly summarized by [55], point to changes in the strength of the Atlantic Meridional Overturning Circulation (AMOC) in phase with Greenland temperatures, with weak (or no) overturning during (Heinrich) stadials and stronger overturning during interstadials (cf. Fig. 1e). An active AMOC is typically thought to have provided the necessary northward heat transport to explain the milder arctic climate during interstadials.

The model proposed here dynamically generates DO events and convincingly reproduces the subsequent interstadial phase in terms of the five features mentioned above as shown in Fig. 1. From a physical modelling point of view, the results presented below suggest that the DO events may have been caused by complex multi-scale interactions between several climate subsystems acting on separate time scales: the ocean circulation, the sea ice, the large-scale atmosphere, and intermittent atmospheric or oceanic events, ordered from slow to fast characteristic time scales.

The paper is structured as follows: We introduce the model in Section 2 and analyze its dynamics in Section 3. We interpret the results in a physical context and also perform a detailed model-data comparison in terms of the above listed five key features. Section 4 discusses the results and relates them to previous analysis. We conclude in Section 5 with a summary of our key findings.

2 Methods

2.1 Monostable excitable model of DO variability

From the slowest to the fastest time scale, the key components of our conceptual multi-scale model are: (i) the Atlantic ocean represented by the meridional temperature and salinity gradients $T(t)$ and $S(t)$ between the Equator and the Nordic Seas, (ii) the Nordic Seas’ sea ice extent $I(t)$, (iii) the Northern Hemisphere atmosphere represented by the meridional temperature gradient $\theta(t)$ and (iv) intermittent oceanic and atmospheric anomalies ξ_t and regular Gaussian atmospheric fluctuations ζ_t . The model set-up is schematically illustrated in Figure 2. For the ease of notation, we will omit the explicit time-dependence of the four dynamical variables in the following; driving noise processes will be subscripted with t . A detailed derivation of the individual model components is provided in the SI Appendix. Here we give only a concise description of the model.

Following the classical Stommel model [56], on the slowest time scale τ_{ocean} the oceanic meridional gradients of temperature and salinity evolve according to

$$\tau_{\text{ocean}} \dot{T} = -\gamma(I)(T - \theta) - (1 + \mu |T - S|)T, \quad (1)$$

$$\tau_{\text{ocean}} \dot{S} = \sigma - (1 + \mu |T - S|)S \quad (2)$$

and determine the strength of the overturning flow

$$q = T - S, \quad (3)$$

representing the AMOC strength [51]. The ocean temperature T is coupled to the atmospheric temperature gradient θ via mutual heat exchange at the (sea ice moderated) rate $\gamma(I)$.

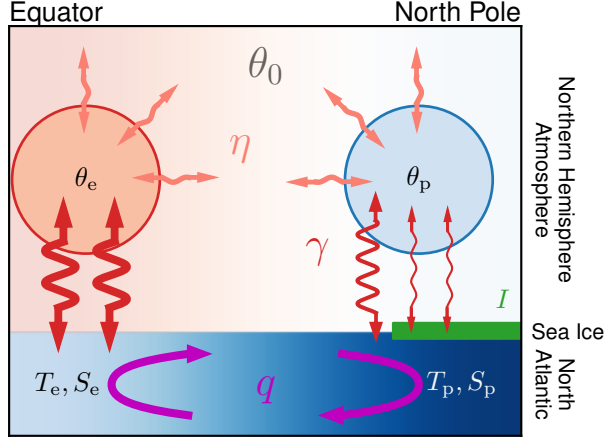


Figure 2: Schematic illustration of the excitable monostable model used to reproduce DO variability of the last glacial. The three key model components are the North Atlantic (bottom), the Northern Hemisphere atmosphere in the North Atlantic region (upper part) and the sea ice in the Nordic Seas (green bar on the right). Oceanic temperature and salinity in the equatorial and polar region are denoted as T_e, S_e and T_p, S_p , respectively. The corresponding meridional gradients follow as $T = T_e - T_p$ and $S = S_e - S_p$. Analogously, the atmospheric temperature gradient $\theta = \theta_e - \theta_p$ is given by the difference between equatorial and polar atmospheric temperatures. A background hemispheric meridional temperature gradient θ_0 is determined by the solar radiation with slow variation driven by changes of the global ice sheet configuration. Atmosphere and ocean exchange heat in both the equatorial and the polar region (dark red arrows). In the polar region the presence of sea ice substantially reduces the heat exchange rate γ . The considered atmospheric polar and equatorial parcels simultaneously dissipate heat (light red arrows) at the rate η such that the meridional atmospheric temperature gradient over the North Atlantic θ relaxes against the background gradient θ_0 . The oceanic gradients T and S translate into a meridional density gradient, that in turn drives the flow q which represents the AMOC. The oceanic salinity gradient S is maintained by constant fresh water flux in the equatorial and polar regions (not shown).

The atmospheric meridional temperature gradient θ relaxes against both a prescribed background state θ_0 and the oceanic gradient T on a fast characteristic time scale $\tau_{\text{atm}} < \tau_{\text{ocean}}$:

$$\tau_{\text{atm}} \dot{\theta} = -\eta(\theta - \theta_0) - \gamma(I)(\theta - T) + \zeta_t, \quad (4)$$

with ζ_t denoting a white noise process that disturbs the atmospheric dynamics. The ratio of the atmospheric redistribution of heat and the atmosphere–ocean heat exchange is set by η .

It is widely accepted that changing background climate conditions strongly influenced DO variability over the course of the last glacial [14–16, 18]. This effect is considered in our model by altering the atmospheric background state θ_0 over time according to

$$\theta_0(t) = 1.59 + 0.23\delta^{18}\text{O}_{\text{LR04}}^*(t), \quad (5)$$

where the normalized benthic stable isotope data $\delta^{18}\text{O}_{\text{LR04}}^*(t)$ is indicative of past global ice volume changes [57]. We argue that a colder background climate increases the atmospheric background temperature gradient θ_0 due to arctic amplification.

On an intermediate time scale τ_{ice} with $\tau_{\text{ocean}} > \tau_{\text{ice}} > \tau_{\text{atm}}$, the temporal evolution of the sea ice is given by the seasonally averaged Eisenman model [58, 59]

$$\tau_{\text{ice}} \dot{I} = \Delta \tanh\left(\frac{I}{h}\right) - R_0 \Theta(I) I - L_0 + L_1 \theta - L_2 I + \xi_t, \quad (6)$$

where $\Theta(I)$ denotes the Heaviside function and the term $L_1 \theta$ represents the influence of the atmosphere on the sea ice formation, with large atmospheric temperature gradients — i.e. colder temperatures at high northern latitudes — fostering sea ice growth and vice versa. The remaining terms represent the ice–albedo feedback, sea ice export and the net incoming and outgoing radiation linearized with respect to I , respectively (see Appendix). The stochastic process ξ_t models fast intermittent random sea ice retreat events that will be explained in greater detail below. The sea ice itself couples back to the ocean and atmosphere dynamics by acting as a dynamic insulator [18, 22] and modifying the respective mutual relaxation rate according to

$$\gamma(I) = \gamma_0 + \frac{\Delta\gamma}{2} \left[\tanh\left(\frac{-(I - I_0)}{\omega}\right) + 1 \right]. \quad (7)$$

In the presence of a stadial sea ice cover ($I > 0.5$) the polar ocean is shielded from the atmosphere and the mutual heat exchange is heavily suppressed. In contrast, a reduced interstadial sea ice cover yields strong atmosphere–ocean heat exchange and correspondingly high mutual relaxation rates.

Although T and θ are gradients, we may compare them directly with observations for oceanic and atmospheric temperature proxies from high northern latitudes, respectively. This is justified since the comparably much larger size of the equatorial region compared to the polar region implies substantially larger heat capacities for the considered equatorial boxes. We thus ascribe changes in the gradients mostly to changes in the polar regions and interpret T and θ as direct counterparts for intermediate and deep ocean temperature proxy records from the Nordic Seas (compare Fig. 1f–g with 1k) and $\delta^{18}\text{O}$ records from Greenland ice cores (compare Fig. 1c with 1h), respectively. The comparison of q with proxies for past AMOC strength is straightforward (compare Fig. 1e with 1j) and so is the comparison of I with proxies for past sea ice extent (compare Fig. 1d with 1i).

Values of the parameters used in our numerical simulation are summarized in Table 1.

2.2 Stochastic (intermittent) forcing processes ξ_t and ζ_t

The deterministic model defined by Eqs. 1–4 and Eqs. 6–7 without a driving force ($\zeta_t = \xi_t = 0$) yields monostable dynamics for $\theta_0 > 1.286$ and is thus as such not suited to model the last glacial’s climate variability. However, it also features a region of slow transitive dynamics located where the nullclines of the atmosphere and sea ice variables are closest (c.f. Fig. 4a and f). We will show later that this meta-stable state in the model’s state space can be identified with interstadial climate conditions of the North Atlantic region. In order to make this meta-stable state accessible to the dynamics we introduce the noise processes ξ_t and ζ_t that

Parameter	Definition	Value
time scales		
τ_{ocean}	oceanic time scale	1000
τ_{ice}	sea ice time scale	200
τ_{atm}	atmospheric time scale	20
atmosphere–ocean model		
γ_0	relaxation rate at full sea ice cover	0.5
$\Delta\gamma$	amplitude of the sea ice’s insolation effect	3.5
η	atmospheric heat dissipation rate	4
μ	flux parameter	7.5
σ	freshwater influx	0.7
sea ice model		
L_0	0th order sea ice OLR	1.3
L_1	linear dependence of sea ice OLR on the atmosphere	1.4
L_2	linear dependence of sea ice OLR on the sea ice	0.35
Δ	strength of sea ice albedo feedback	0.25
h	characteristic sea ice albedo feedback scale	0.08
R_0	rate of sea ice export	0.4
ω	characteristic insulation scale of sea ice	0.8
I_0	sea ice value, at which half of the insulation effect is reached	-0.5

Table 1: Model parameters used in all simulations, unless stated otherwise. The parameters are chosen to reproduce the key features of DO events.

mimic the effect of unresolved events occurring on time scales faster than the characteristic time scales τ_{ice} and τ_{atm} of the sea ice and atmosphere dynamics, respectively.

The atmosphere variable θ is assumed to be subjected to Gaussian white noise forcing $\zeta_t = \sigma_\theta \dot{W}$ with standard Brownian motion W . This noise can be motivated as the effective stochastic effect of unresolved strongly chaotic atmospheric fluctuations on θ [60]. This noise does not substantially affect the dynamics of Eqs. 1–4 and Eqs. 6–7 but generates more realistic fluctuations of θ in accordance with the NGRIP $\delta^{18}\text{O}$ record.

The sea ice noise ξ_t , however, will play a major role in triggering DO events. To generate rare but large forcing events which allow the system to leave the stadial fixed point and enter the meta-stable state, non-Gaussian noise is required. [51] showed that α -stable noise, which is characterized by the occurrence of discrete jumps, can be dynamically generated in a multi-scale setting to produce abrupt warming events in a Stommel model driven by a simple sea-ice model. Here, we postulate that sea ice is subjected to rare and intermittent fast processes. According to the theory laid out in [61–63] and [51], this forcing, when integrated, gives rise to an effective α -stable component in the resulting dynamics of the sea ice. By controlling the heat exchange rate $\gamma(I)$ the sea ice in turn drives the atmospheric and oceanic variables θ and T with emergent non-Gaussian noise. Indeed, signatures of non-Gaussian α -stable noise have been detected by [44] in the calcium concentration record of the GRIP ice core [64].

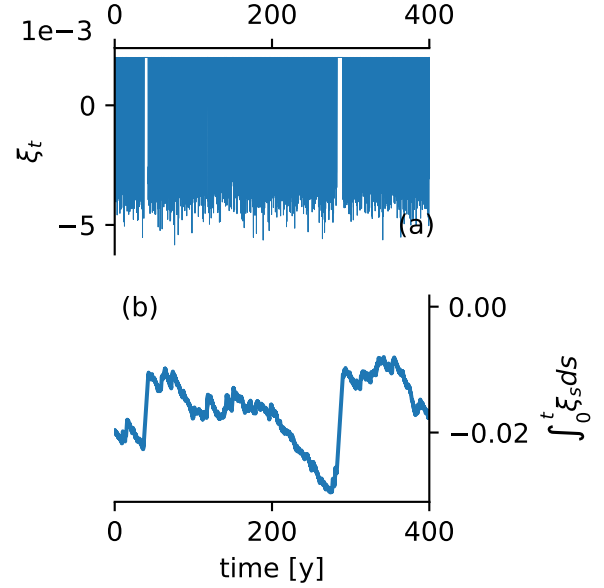


Figure 3: Illustration of the driving noise process ξ_t acting on the sea ice (a) and its integrated form $\int_0^t \xi_s ds$ (b). It is clearly seen how prolonged laminar phases of the driving noise ξ_t result in jumps in the integrated $\int_0^t \xi_s ds$. These jumps may translate into supercritical sea ice removals and trigger DO events in our excitable model.

We propose two possible physical mechanisms which may constitute such intermittent forcing on the sea ice: oceanic convective events and atmospheric anomalies. During stadials, the Nordic Seas’ sea ice is shielded from the warmer subsurface and deep waters by a thin layer of cold and fresh water [20, 22]. We hypothesize that intermittent convective events may temporarily remove this layer and melt sea ice from below, efficiently opening up polynia through which oceanic heat could be released to the atmosphere [39]. Either, after locally releasing sufficient heat, a stable stratification of the ocean reestablishes and the polynia refreeze. Or, the convective events might remove a critical amount of sea ice and push the system into the meta-stable interstadial state.

Strong atmospheric anomalies constitute another possible source of intermittent sea ice forcing. [65] and [66] describe — although in a somewhat different setting — how persistent atmospheric anomalies can drive the high northern latitude climate into a substantially altered state.

We postulate that the mechanisms giving rise to intermittent anomalous forcing events are active only during stadials. During interstadials, convectively driven sea ice removal should not have a strong impact on the already northward displaced sea ice edge, because the warm Atlantic inflow loses too much heat before it could be subdued under the sea ice. Similarly, we argue that atmospheric anomalous forcing events require a certain meridional temperature gradient and a stadial configuration of the jet stream. Therefore, we impose a Gaussian white noise forcing of the sea ice dynamics with $\xi_t = \sigma_I \dot{W}$ with standard Brownian motion W if no pronounced stadial sea ice cover is present ($I < 0.5$). Since sea ice fluctuations are smaller, the smaller the sea ice extent, we choose relatively

Parameter	Definition	Value
atmospheric noise ζ_t		
σ_θ	amplitude of the atmospheric noise	0.04
sea ice noise ξ_t during stadials		
c	laminar forcing strength	0.2
σ_Ω	amplitude of the Brownian motion during turbulent phase	0.01
$k = 1/\alpha$	shape parameter of Pareto distribution	0.62
σ_Σ	scale parameter of the Pareto distribution	2
$\mu_\Sigma = \sigma_\Sigma/k$	location parameter of the Pareto distribution	3.2
sea ice noise ξ_t during interstadials		
σ_I	amplitude of interstadial Brownian motion	0.006

Table 2: Parameters for the stochastic processes ζ_t and ξ_t which drive the atmosphere and sea ice in 4 and 6, respectively.

small σ_I as compared to the sea ice fluctuation emerging from the more complex stadial driving noise which we describe in the following.

To model intermittent convective events or atmospheric anomalies, we follow [61, 62] and design a (mean-zero) process which consists of a succession of turbulent and laminar periods. The forcing in the laminar periods is set to a constant $\xi_t = -c$ whereas during the turbulent periods it fluctuates around $\xi_t = c$ according to standard Brownian motion with $\xi_t = c + \sigma_\Omega \dot{W}$. The respective durations of these phases are themselves random variables. In particular, durations of the laminar period Σ can be arbitrarily long and are distributed according to a Pareto law

$$\Sigma \sim \frac{1}{\sigma_\Sigma} \left(1 + k \left[\frac{\Sigma - \mu_\Sigma}{\sigma_\Sigma} \right] \right)^{-(1/k+1)} \quad (8)$$

with shape parameter $k = 1/\alpha$, scale parameter σ_Σ , and location parameter $\mu_\Sigma = \sigma_\Sigma/k$. Hence, laminar periods last on average for $\mathbb{E}[\Sigma] = \sigma_\Sigma \alpha^2 / (\alpha - 1)$ time units (assuming $\alpha > 1$). The durations of turbulent periods Ω are uniformly distributed around the mean $\bar{\Omega} = \mathbb{E}[\Sigma]$ with $\Omega \sim \bar{\Omega} + U[-\bar{\Omega}/2, +\bar{\Omega}/2]$, where $U[a, b]$ denotes the uniform distribution between the limits a and b . When such a process is integrated, the laminar periods yield ballistic flights $\sim -c\Sigma$. The heavy tail of the Pareto distribution assigns a probability of $(\alpha\sigma)^\alpha \vartheta^{-\alpha}$ to durations $\Sigma > \vartheta$, and allows for $\alpha < 2$ for non-vanishing probabilities of ballistic flights of arbitrary lengths. This renders $\int \xi_t dt$ an effective α -stable process. This mechanism of intermittent laminar dynamics generating α -stable noise is illustrated in Figure 3, where we show the stochastic process ξ_t and its integrated form.

Long lasting laminar forcing events may remove large amounts of sea ice and thus entail an abrupt shift in the atmosphere–ocean heat exchange which determines the climatic state of the coupled atmosphere–ocean model (cf. Fig. 4). Such dynamically generated perturbations are capable of inducing meta-stable interstadial dynamics in our model as we will show in the next section. In Table 2 we list the parameters used to generate the noise.

3 Results

In this section we will first analyze the response of the deterministic coupled model to imposed perturbations of the sea ice cover with $\zeta_t = \xi_t = 0$ and a constant climate background temperature θ_0 . We show that long lasting interstadial-like excursions occur as a consequence of supercritical sea ice perturbations of the stable stadial state. This phenomenon results from a complex interplay of the three separate time scales and the slow deterministic dynamics in a particular meta-stable region of the state space, which is characterized by high proximity of the θ and I nullclines (cf. Fig. 4). We then show that the intermittent noise ξ_t is capable of generating such supercritical perturbations to the sea ice acting as triggers of interstadials. Finally, the full stochastic model, coupled to the background climate, is run over the entire last glacial.

3.1 Deterministic response to sea ice perturbations

To understand how our model may explain DO variability, we investigate how the deterministic system given by Eqs. 1–4 and Eqs. 6–7 with $\zeta_t = 0, \xi_t = 0$ recovers after large imposed perturbations of the sea ice variable for two different choices of θ_0 , corresponding to warm and intermediate glacial climate backgrounds, respectively (Fig. 4). In simulations initialized in the stadial stable state, at time $t_p = 200$, the sea ice is abruptly removed by manually setting $I(t) = I_p$ with $I_p = \{0.2, 0, -0.2, -0.5, -1, -2\}$. Subsequently the system evolves freely and relaxes back to the unique stadial fixed point. The character of the relaxation depends on the strength of the perturbation as well as the value of the climate background θ_0 . We observe distinct phases in the system response which shall be discussed separately in the following.

Phase A: immediate atmospheric response. Since on small time intervals the slow ocean dynamics T and S can be considered as constants for the faster atmosphere dynamics θ , the atmosphere rapidly increases to the value θ_p (see Fig. 4b,g), which is approximately given as the solution to $\gamma(I_p)(\theta_p - T_s) + \eta(\theta_p - \theta_0) = 0$ (shown as a light orange line in Fig. 4 as a guide to the eye), where the subscript s denotes the respective stadial fixed point values. Physically, θ_p is determined as the balance of atmospheric uptake of oceanic heat $\gamma(I_p)(\theta_p - T_s)$ and its associated atmospheric redistribution (dissipation) $\eta(\theta_p - \theta_0)$ in response to the sudden exposure to a warm stadial ocean (small T) which was previously shielded from the atmosphere by the stadial sea ice cover. The slow model time scale τ_{ocean} may in this context be interpreted as the large heat capacity of the Nordic Seas, allowing them to release heat to the atmosphere while remaining themselves unchanged on short time scales.

Phase B: system-wide relaxation. We now discuss how the system relaxes from the perturbed state $(\theta_p, T_s, q_s, I_p)$ back to the unique stable fixed point $(\theta_s, T_s, q_s, I_s)$. Notice that the sea ice bifurcation point I_{B2} marks the lowest sea ice cover of the sea ice nullcline’s stable branch with reduced sea ice cover (cf. Fig. 4). The relaxation is qualitatively different depending on whether the perturbation brings the sea ice to the low-ice regime ($I_p < I_{B2}$) or not. If that is the case, the system takes a prolonged excursion in state space with a two-stage relaxation process, of which the first stage can

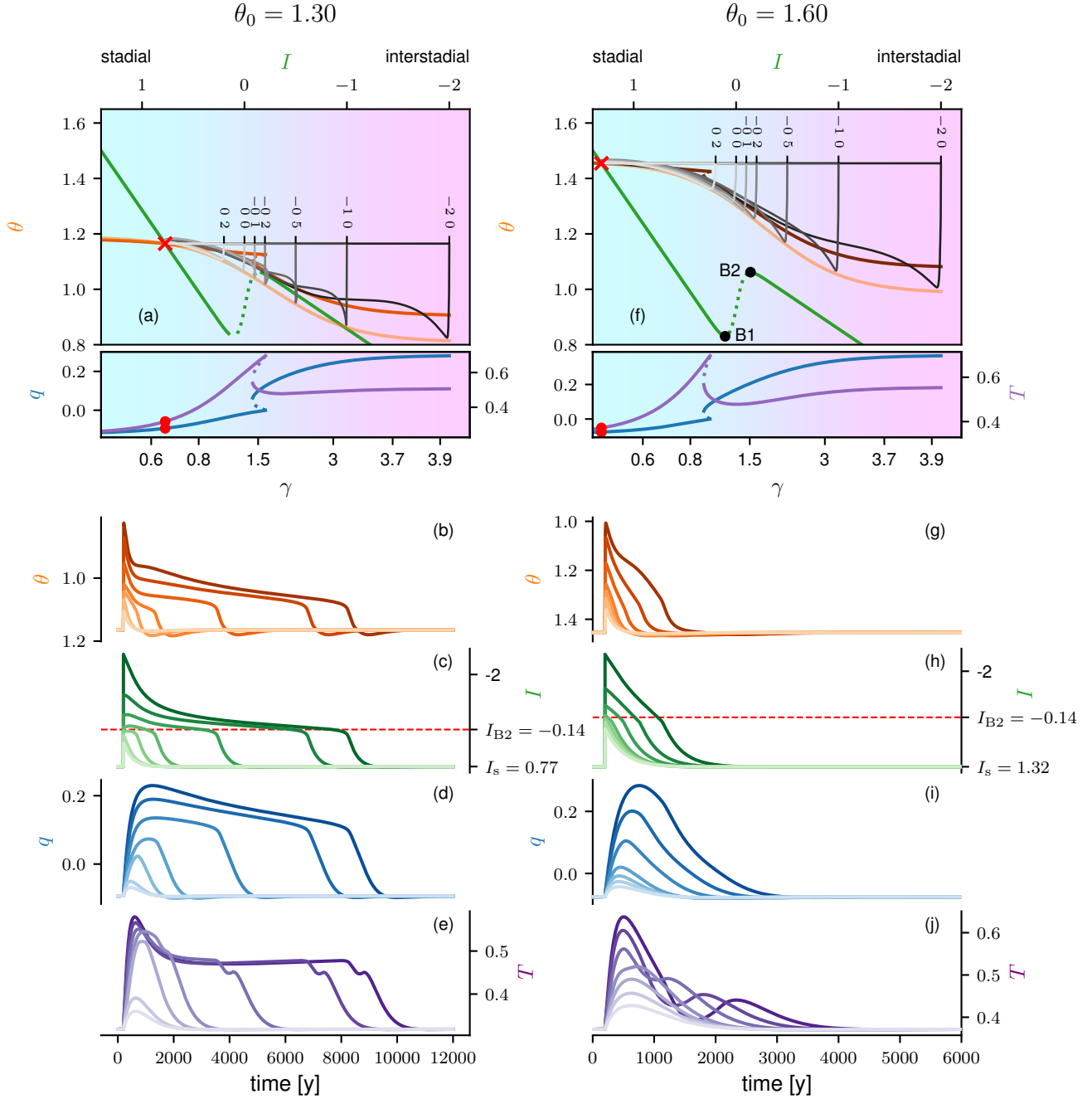


Figure 4: Trajectories of the deterministic system defined by Eqs. 1–7 subjected to instantaneous sea ice retreat at $t = 200$ for several values of the perturbed sea ice state $I_p = \{0.2, 0.0, -0.2, -0.5, -1.0, -2.0\}$ (gray horizontal lines in a and f). In panels (a–e) $\theta_0 = 1.3$ (warmer background climate) while in panels (f–j) $\theta_0 = 1.6$ (colder background climate). (a) and (f) show the trajectories in the θ – I plane together with the corresponding nullclines of all four model variables. A prescribed value for the sea ice variable (top axis) determines the atmosphere–ocean heat exchange rate γ (bottom axis), which in turn sets the fixed points of θ , T and q . Strong sea ice cover and a low heat exchange rate yield a cold polar atmosphere (large θ), warm intermediate and deep waters in the Nordic Seas (small T) and a weak AMOC (small $|q|$). This configuration corresponds to stadial climate conditions as inferred from proxy records. A small sea ice cover reversely entails a warm polar atmosphere (small θ), cold Nordic Seas (large T) and an active AMOC (large $|q|$) which can be identified with interstadial climate conditions. Since θ couples back to the sea ice I , intersections of the I - and θ -nullcline constitute fixed points of the entire system in the θ – I plane (red cross) with values for T and q (red dots) following from the heat exchange rate associated with this intersection. All trajectories are initialized at the unique stable fixed point. The remaining panels show the trajectories of the individual system variables against time for the different sea ice perturbations. The horizontal dashed lines in panels (c) and (h) mark the critical sea ice threshold I_{B2} which constitutes the highest possible sea ice cover in the low-ice regime. Vice versa, the other sea ice bifurcation point I_{B1} marks the lowest possible sea ice cover in an ice-rich regime viewed in the θ – I plane.

be identified with interstadial climate conditions. We call this scenario, which involves responses of all model variables, the supercritical case. If $I_p > I_{B2}$, then the system shows a straight relaxation back to stadial conditions without any substantial response of the oceanic variables to the initial perturbation. We term this scenario the subcritical case. The existence of both subcritical perturbations which rapidly relax back to the steady state and supercritical perturbations which cause long transitory dynamics back towards the steady state involving several time scales is a hallmark of so called excitable media often found in neurophysiological systems.

Phase B: subcritical case $I_p > I_{B2}$. In the subcritical case the system remains in an ice-rich state which due to the albedo feedback facilitates a fast regrowth of the sea ice. Consequently, the dynamics of I and θ jointly relax back straight to the stadial equilibrium as the regrowing sea ice increasingly shields the atmosphere from the warmer ocean. The oceanic variables on the other hand show hardly any response due to their higher inertia and the fast sea ice recovery. Qualitatively the general system response to subcritical perturbations is the same for $\theta_0 = 1.3$ and $\theta_0 = 1.6$.

Phase B: supercritical case $I_p < I_{B2}$ - Stage 1. In contrast, in the supercritical case a phase of slowed-down sea ice recovery occurs, giving the oceanic variables enough time to respond to the perturbation such that all model variables temporarily assume interstadial configurations, i.e. in addition to the elevated arctic atmospheric temperature (low gradient θ) and the reduced Nordic Seas' ice cover (low I), the AMOC assumes its strong circulation mode (large q) and the Nordic Seas cool at intermediate and large depth (high gradient T) in agreement with proxy evidence (cf. Fig. 1).

As a consequence of the substantially reduced sea ice cover the ice-albedo feedback now inhibits the reformation of the sea ice and in the presence of warm atmospheric conditions θ_p the sea ice regrows at a slow rate towards I_{B2} or retreats even further. As the atmosphere continuously dissipates the heat it receives from the ocean, the latter starts to notably cool (increase in T). In turn, the oceanic cooling reduces the atmospheric uptake of oceanic heat and as a result the arctic atmosphere cools in parallel (pronounced increase in θ in Fig. 4 shortly after the perturbations). This effect inevitably prevents a stabilization of the system in the low-ice regime and ensures that the sea ice eventually regrows. A second consequence of the Nordic Seas' cooling is the transition of the AMOC from a salinity-driven weak mode to the temperature-driven strong mode. This completes the interstadial configuration of the four model variables and allows us to identify this first stage of the supercritical relaxation with the interstadial climate. Fully reactivated, the AMOC's northward oceanic heat transport stabilizes the temperatures of the Nordic Seas and over the course of the remaining interstadial the slow adjustments of the other variables are driven by the incremental sea ice regrowth.

The nature and duration of the interstadial stage depends on both the size of the initial sea ice perturbation I_p and the closeness of the sea ice nullcline and the atmosphere nullcline. If the two nullclines are close (as for $\theta_0 = 1.3$) the dynamics of θ and I is comparably slow (cf. the dynamics for $\theta_0 = 1.3$ in Fig. 4). Sufficiently strong sea ice perturbations then result

in pronounced interstadials during which all system variables hardly change over an extended period of time. If the nullclines are further apart (as for $\theta_0 = 1.60$) the interstadial state is less pronounced and characterized by continuous change in all model variables, driven by steady sea ice regrowth.

Phase B: supercritical case ($I_p < I_{B2}$) - Stage 2. Once the sea ice has regrown past I_{B2} , its further regrowth accelerates substantially, marking the beginning of the second stage in the supercritical system-wide relaxation process. This is due to the strongly changing albedo effect around intermediate sea ice cover. The regrowing sea ice increasingly prevents oceanic heat loss to the atmosphere, which entails polar atmospheric cooling and initiates warming of the Nordic Seas. The reduction of the oceanic temperature gradient is closely followed by a corresponding reduction in the AMOC strength. Since the atmosphere equilibrates quasi-adiabatically to the declining heat exchange rate $\gamma(I)$, it cools at the same accelerated rate as the ice recovers and both atmosphere and sea ice reach stadial configuration within a few hundred years after the sea ice passed its threshold I_{B2} . The oceanic variables follow with some inertia; they exhibit a sustained relaxation after the faster atmosphere and sea ice have already clearly transitioned to their stadial configuration. This second stage of the supercritical relaxation process corresponds to the abrupt interstadial-stadial transitions observed in the paleoclimate record.

3.2 Noise-driven interstadials

We now show that the intermittent driving noise ξ_t is able to generate large sea ice perturbations which may trigger DO events provided they are supercritical. Fig. 5 shows trajectories of the dynamics determined by Eqs. 1–4 and Eqs. 6 and 7 under the influence of the driving noises ξ_t and ζ_t with a constant atmospheric background climatic state θ_0 . Overall there is high visual agreement between simulated θ trajectories (Fig. 5) and the DO cycles recorded in the NGRIP $\delta^{18}\text{O}$ data (Fig. 1a and c).

For $\theta_0 = 1.3$ the θ -trajectory resembles DO cycles from the early glacial, with two persistent interstadials separated by a short stadial. For $\theta_0 = 1.6$ the θ -trajectory has a greater similarity with the mid to late glacial, with shorter interstadials and predominantly stadial conditions. Confirming the discussion in the previous section, interstadials last longer and have a more pronounced plateau in all variables for the smaller atmospheric background temperature gradient $\theta_0 = 1.3$. Moreover, a subtle increase in the stadial duration can be observed for larger θ_0 . The colder stadial conditions associated with larger θ_0 imply an increased distance between the sea ice's stable stadial configuration I_s and the critical sea ice threshold I_{B2} . Hence, for unchanged driving noise ξ_t , the probability for the noise to drive the system across I_{B2} is reduced for larger θ_0 and thus the waiting time between two supercritical stochastic forcing events is higher and the stadials are longer. However, this effect is attenuated by the fact that DO events can also be triggered by two pronounced yet subcritical laminar forcing periods in quick succession.

The noise process ζ_t driving the θ variable blurs the exact timing of DO cooling transitions in agreement with $\delta^{18}\text{O}$ ice

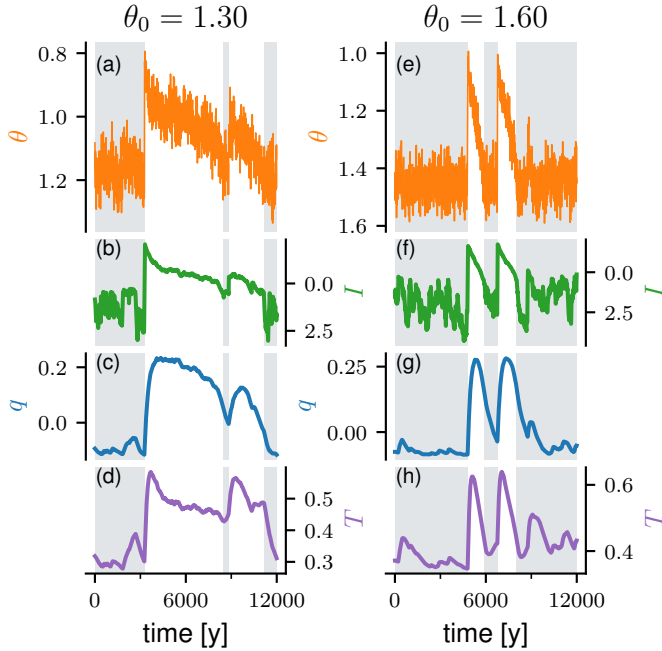


Figure 5: Trajectories of the model system defined by Eqs. 1–7 driven by the noise scheme as described in Sect. 2.2, i.e., with non-zero noise ζ_t and ξ_t , for $\theta_0 = 1.3$ (left column) and $\theta_0 = 1.6$ (right column). The gray shading indicates stadial intervals. A DO event is defined by at least 25 consecutive years of sea ice cover $I > I_{B2}$ within a stadial followed by at least 15 years of reduced sea ice cover of $I < I_{B2}$. Provided that the system is in an interstadial state, the reverse interstadial-stadial transition occurs when the sea ice regrows past $I_c = 0.5$ and maintains this level in an average over the following 25 years. The hysteresis in the definition of climate transitions prevents a jumping back and forth between the two states when the sea ice fluctuates close to a potential critical threshold and gives rise to well defined climatic periods.

core records. In the sea ice, however, these transitions are still fairly distinct. Compared to the deterministic setup, sea ice perturbations of the same strength yield shorter interstadials. This behavior occurs, because the delicate balance of influences that yields the slow sea ice regrowth of the meta-stable interstadial is highly susceptible to small sea ice fluctuations. The latter may easily push the system across the critical threshold of I_{B2} and thereby immediately end the interstadial.

Remarkably, our model reproduces several irregular features of the original $\delta^{18}\text{O}$ record, with respect to variability in terms of shape, duration, and amplitude of DO cycles. The different strengths of the sea ice perturbations translate into different lengths of the interstadial intervals for given background conditions. Also, the first interstadial of the $\theta_0 = 1.3$ trajectories shows what resembles an overshoot, i.e. a pronounced peak in the arctic atmospheric temperatures that decays rapidly over the first quarter of this interstadial. Overshoots similar to this one can be observed for example at the beginning of interstadial 20c or at the beginning of interstadial 1 in the NGRIP record [12]. Both trajectories exhibit pronounced perturbations within a stadial towards a warmer arctic atmosphere that do not develop into a full interstadial. Perturbations of

this kind can also be found in the NGRIP record.

3.3 Realistic climate background

Finally, we run a simulation of the last glacial with the full model defined by Eqs. 1–7 with a changing atmospheric background climate (Fig. 6). With the linear coupling to the LR04 $\delta^{18}\text{O}$ stack introduced in Eq. 5 the atmospheric background state θ_0 assumes low values around 1.3 during the early parts of the last glacial and increases to high values $\theta_0 > 1.9$ around the last glacial maximum. As discussed in Sect. 3.1 and 3.2, this leads to longer lasting interstadials during the early glacial and shorter ones during the late glacial, with the opposite effect although much less pronounced for stadials. Hence, the predominance of long lasting interstadials with only short stadial inceptions in the early glacial is reversed towards the late glacial (cf. Fig. 6). In general, the time scales of the stadials and interstadials match those observed in the proxy data throughout the entire last glacial. During the very cold conditions toward the end of the last glacial, DO events are unlikely but not impossible to occur in our simulations.

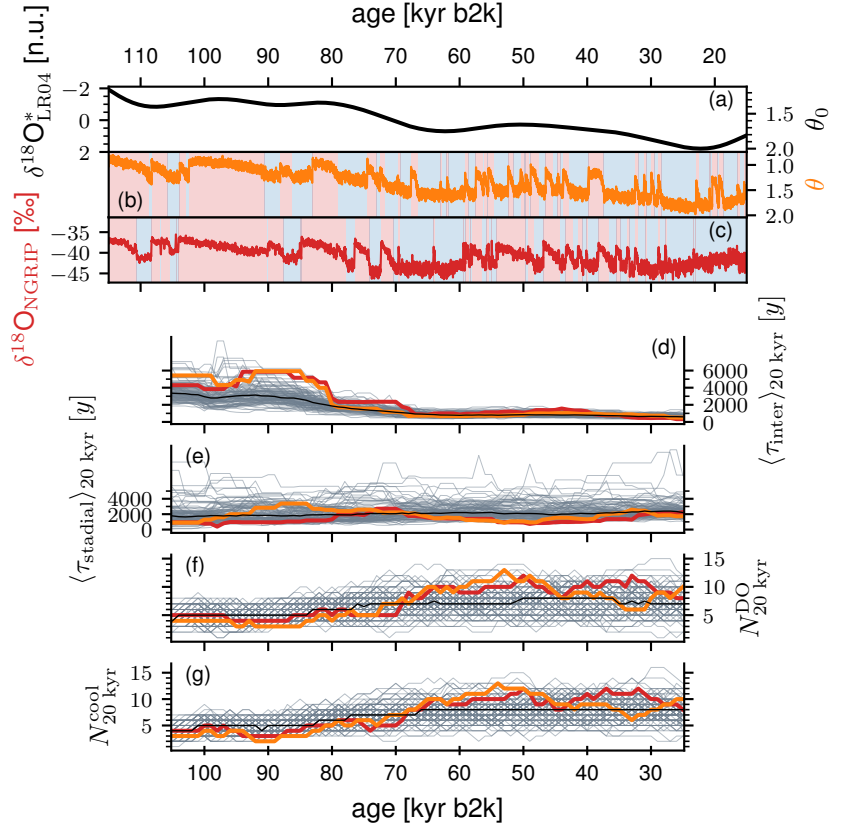
4 Discussion

Overall, the modelled atmospheric temperature θ resembles the NGRIP $\delta^{18}\text{O}$ record over the entire last glacial in terms of shape and periodicity of DO cycles (compare Fig. 1a with b). The general features of strong (reduced) sea ice cover, weak (strong) AMOC and warm (cold) Nordic Seas during stadials (interstadials) are likewise consistently reproduced by the model (compare Fig. 1c–g with h–k).

We now discuss the similarity between proxy records and our simulations with focus on the five key characteristics of DO variability as listed above, which rely on a multitude of proxy records of ocean, ice core, and terrestrial origin [20, 22, 24, 26, 49, 52, 55, 67].

1. **Shape of DO cycles:** The general shape of the DO cycles is reproduced well by the modelled atmospheric temperature θ (Fig. 1a,c vs. Fig. 1b,h). Our model also resolves several finer-scale features of the proxy record of the last glacial, such as precursor events – short-lived strong positive excursions in the $\delta^{18}\text{O}$ data that do not evolve into full interstadials such as interstadial 5.1 at ~ 31 kyr b2k or interstadial 16.2 at ~ 58 kyr b2k (Fig. 1b and Fig. 6) or very short stadial inceptions similar to the stadial 23.1 at ~ 90 kyr b2k and the stadial 21.2 at ~ 85 kyr b2k which yield apparent back-to-back interstadials [12]. Furthermore, consistent with the proxy record, several interstadials exhibit a continuous trend of moderate cooling back to full stadial conditions instead of the more typical abrupt final cooling.
2. **Duration of stadials and interstadials:** The modelled variability of stadial and interstadial durations is in good agreement with the data (cf. Fig. 6). In our simulations the coupling of the background climate θ_0 to the LR04 benthic $\delta^{18}\text{O}$ introduced in Eq. 5 causes a gradual transition from predominantly interstadial to predominantly stadial climate across the last glacial due

Figure 6: Simulation of the period 115–15 kyr b2k of the full stochastic model given by Eqs. 1–7 with the coupling to the background climate. (a) 50 kyr low-pass filtered LR04 benthic $\delta^{18}\text{O}$ stack in normalized units. The right-hand-side ordinate indicates the corresponding $\theta_0(\delta^{18}\text{O}_{\text{LR04}}^*)$ according to Eq. 5. (b) Simulated trajectory of θ as a direct model counterpart of the NGRIP $\delta^{18}\text{O}$ record. The effect of the changing θ_0 on the interstadial duration and to a lesser extent on the stadial duration is apparent, with a predominance of long interstadials in the earlier part of the glacial and only short interstadial excursions from mostly stadial climate during the late glacial. (c) NGRIP $\delta^{18}\text{O}$ data as in Fig. 1a. (d) The duration of occurring interstadials averaged in a 20 kyr running window $\langle\tau_{\text{inter}}\rangle_{20 \text{ kyr}}$ for the proxy data (red) and the simulation (orange) and for 99 alternative realizations of the simulation (gray). The black line indicates the average over all 100 model runs. The 20 kyr mean duration takes into account all interstadials that are either fully included in the window or that end or start within the window. Interstadials that stretch across the window boundaries are considered with their full duration. (e) Same as (d) for the 20 kyr running mean duration of stadials $\langle\tau_{\text{stadial}}\rangle_{20 \text{ kyr}}$. (f) Number of DO events occurring in a 20 kyr running window $N_{20 \text{ kyr}}^{\text{DO}}$ with the same color coding as before. (g) The same as (f) for the number of DO cooling events $N_{20 \text{ kyr}}^{\text{cool}}$.



to the mechanisms explained in Sects. 3.2 and 4. The slow variations in the overall stadial and interstadial levels are reproduced by our simulations, however with an apparent mismatch prior to the last glacial maximum, where the NGRIP $\delta^{18}\text{O}$ record shows a persistent warming trend (within a stadial climate), while our simulation evolves to colder temperatures (cf. Fig. 6). This mismatch originates from the fact that the warming trend in the NGRIP record is in contrast to the global cooling trend prior to the last glacial maximum [68].

3. **In-phase sea ice dynamics:** The extensive (minimal) sea ice cover during stadials (interstadials) suggested by proxy records [20, 22, 52, 69] is well reproduced by our model; the sea ice I consistently regrows at a moderate rate over the course of the interstadial, before it returns to its stadial extent in a final phase of accelerated regrowth marking the interstadial–stadial transition. Overall, this behavior agrees with the sea ice dynamics in the Nordic Seas across DO cycles as inferred by [20] and others. While proxy records suggest a continued sea ice growth during the early stadial, the modeled sea ice I reaches its stadial extent already during the interstadial–stadial transition and the regrowth thus does not stretch significantly into the stadial phase.
4. **Nordic Seas’ temperature inversion:** In our interpretation of the modeled oceanic temperature gradient T we ignore surface waters and regard T as an indicator

of subsurface and deep water temperatures. Indeed, our model simulates warm Nordic Seas at full stadial conditions (Fig. 1k), in line with the proxy records [22, 24, 49]. At the beginning of interstadials, pronounced cooling sets in, which can be interpreted as a continuous convection-driven release of the heat previously stored underneath the sea ice cover. Approximately one third into an interstadial the subsurface cooling is reversed into a more gentle yet persistent warming trend caused by regrowing sea ice and decreasing heat loss which accelerates across the transition back to stadial conditions, but is sustained in the subsequent stadial. In general, this pattern agrees very well with existing paleoclimate proxies [20, 22, 24, 49]. The moderate warming that persists over the final two thirds of the interstadial can be observed in a very similar manner in the benthic $\delta^{18}\text{O}$ from marine sediment cores indicative of deep ocean temperatures (compare Fig. 1g with Fig. 1k). The deep ocean warming is attributed to a gradual reduction of deep convection over the course of the interstadial driven by regrowing sea ice [20, 24]. Conversely, the subsurface temperature reconstructions (Fig. 1f) reveal a mild cooling trend during this phase of the DO cycle, which is not reproduced by the model. Subsequent to the interstadial–stadial transition the observed sustained warming of the intermediate and deep ocean into stadials is reproduced by our model, where a salinity driven stadial AMOC ($q < 0$) counteracts an existing meridional temperature gradient and the sea ice

cover prevents heat loss to the atmosphere.

5. **AMOC switches:** The correspondence between strong (weak) overturning and interstadial (stadial) climate conditions is widely accepted [21, 26, 35, 36, 39, 55, 70]. However, limited quality of the proxy data prevents a more detailed assessment of the changes in the AMOC during the course of a typical DO cycle. It seems that the AMOC almost stopped during Heinrich stadials, while during non-Heinrich stadials it probably operated in a weak and shallow mode [55]. An AMOC reinvigoration is reported to have happened in synchrony with abrupt Greenland warmings, within the limits of dating uncertainties [55]. In general terms, simulated changes of the AMOC strength agree with this pattern apart from the specific expression of Heinrich events, which aren't explicitly targeted by our modeling setup (c.f. Fig. 1e and j). From the interstadial onsets onward the AMOC strength increases until it plateaus somewhere half way through the interstadial. Thereafter a weakening trend sets in whose strength is related to the climate background condition and which stretches well into the stadial before the AMOC recovers its stadial state.

Our four-dimensional model given by Eqs. 1–7 hence reproduces central features of DO variability in terms of arctic temperatures θ , Nordic Seas' sea ice cover I , intermediate-to-deep water temperatures T , and the meridional overturning strength q . In particular, our modelling results align well with the characteristics of DO variability inferred from the study of marine sediment cores from the northern North Atlantic and the Nordic Seas [20, 22, 24, 49, 52, 67, 71]. First pointed out by [67, 71] a sustained inflow of North Atlantic warm water into the Nordic Seas during stadial periods was later confirmed and integrated in a conceptual explanation for the emergence of DO variability by [49]: The sustained inflow of warm and salty waters during stadials is subdued under a strong halocline which eventually separates a cold and fresh surface layer from the intermediate and deep waters. These experience a gradual warming up to the point where the growing vertical temperature gradient destabilizes the stratification and (re)initiates deep convection. This in turn reinvigorates the AMOC and cools the intermediate to deep waters in the Nordic Seas. The transition back to the stadials is more or less explicitly attributed to the prevailing glacial climate background conditions [49]. [22] and later [20] supplemented this framework by providing observational evidence for extended (reduced) Nordic Seas' ice cover during stadials (interstadials), highlighting the role of the sea ice as an insulator between atmosphere and ocean. Our model shows remarkable agreement with corresponding proxy evidence (compare Fig. 1) and integrates well into the above narrative. The insulating effect of the sea ice, which has previously also been considered by [18] as a crucial component, is modeled explicitly in our study and is confirmed to be key to the changes between stadial and interstadial climates. The observed sustained stadial inflow of warm North Atlantic waters into the intermediate depth Nordic Seas corresponds to a weak, salinity-driven AMOC in our model. Importantly, in contrast to the majority of previous work but in agreement with the above, in our model

interstadials do not correspond to stable fixed points, but rather to meta-stable states that inevitably relax back to stadial climate conditions.

However, our view of DO cycles as an excursion triggered by supercritical perturbations in an excitable medium provides a new aspect to the above narrative: The continued warming of the intermediate waters as described by [49], [22], and [18] would inevitably trigger the next DO event in a finite amount of time. According to our model, the stadial climate is stable and could persist for very long time if no supercritical forcing event occurred. In line with this, [20] suggest that DO-triggering destabilizations of the stadial halocline might have been triggered themselves by elevated Atlantic inflow, caused by stochastic atmospheric action on the subpolar gyre [40, 72]. Our model does not resolve the exact triggering mechanism and instead relies on intermittent noise, which may trigger DO events by removing sufficiently large amounts of sea ice reactivating atmosphere–ocean interaction in the high latitudes. So far, as a source of this noise, we have proposed either atmospheric anomalies as described by [65] and [40] or, inspired by [20], [22], and [49] convective events in the ocean. The interplay of both mechanism as suggested by [20] might even be better suited to justify the choice of our driving noise.

Apart from its central role as the DO event trigger, we find that the intermittent driving noise can indeed explain several details of the NGRIP $\delta^{18}\text{O}$ record; the variable strength of the supercritical perturbations translates into a variability in terms of shape and duration of interstadials. The reproduction of back-to-back interstadials with no extended stadial separating them as well as very short interstadials follows naturally from the stochastic nature of the trigger in our simulation. Similarly, the variability of stadial durations results in our model from randomly distributed waiting times between supercritical perturbations. Taking all these arguments together, we find a purely deterministic mechanism of DO events to be more difficult to reconcile with the variable expression of interstadials in the proxy records. Furthermore, subcritical forcing events contribute to the higher fluctuations of the stadial arctic atmospheric temperatures as compared to the interstadial one in our simulation which is also observed in the NGRIP $\delta^{18}\text{O}$ record. These subcritical events could be interpreted as local convective events that entail a partial and temporary removal of stadial sea ice associated with the release of a certain amount of oceanic heat.

It should be noted that the three different time scales introduced together with the dynamical equations for the three model components are crucial to obtain agreement between the modeled and the observed shape and duration of DO cycles. The other key ingredient for the successful simulation of sustained interstadial intervals is the proximity of the θ and ice nullclines, which gives rise to an additional slow time scale and a meta-stable state. The existence of such a meta-stable state, whose expression is highly sensitive to background conditions, seems physically plausible in view of a delicate interplay between northward oceanic heat transport, the high latitude atmospheric temperatures and the ice-albedo feedback. The influence of warm Atlantic surface inflow in the Nordic Seas on the formation of sea ice during interstadials

has so far been neglected, but should be considered in further research.

5 Conclusions

In summary, we have modeled DO cycles across the last glacial period as state space excursions of an excitable monostable system, resolving the ocean, sea ice and atmosphere on increasingly fast time scales. DO events are triggered by an intermittent noise scheme that acts on the stadial sea ice cover. The associated effect on the atmospheric Arctic temperatures θ is consistent with the observed α -stable noise signature in the GRIP calcium record [44]. We propose as potential sources for the driving intermittent noise local and temporary convective instabilities in the stadial stratification of the Nordic Seas [73, 74] or persistent atmospheric anomalies [40, 65], or combinations thereof [20]. Our model reproduces the observed DO cycle patterns of four climate variables central to the physics of DO cycles: the typical saw-tooth shape of arctic atmospheric temperatures [1, 7], the reduced (extended) sea ice cover during interstadials (stadials) [20, 22, 52, 69], the strong interstadial AMOC, with sustained northward heat transport during stadials at a weaker level [22, 49, 55, 67], and the corresponding stadial warming of the Nordic Seas [20, 22, 24, 49]. Furthermore, detailed aspects of the NGRIP $\delta^{18}\text{O}$ record, such as the variability of the interstadial shape and duration, higher-amplitude stadial fluctuations, and very short interstadials (stadials) during the colder (warmer) parts of the late glacial, are reproduced.

Here, we summarize the most important features of our model that provide plausible mechanistic explanations to the last glacial’s millennial-scale climate variability:

1. The rate of ocean–atmosphere heat exchange in the high northern latitudes is decisive for the state of the North Atlantic climate system. The heat exchange is controlled by the sea ice.
2. Stochastic removal of the sea ice may abruptly expose the atmosphere to the influence of a large oceanic heat reservoir and entail abrupt atmospheric warming and oceanic cooling facilitated by reactivated deep convection. The latter happens at a much slower rate due to the ocean’s much larger heat capacity.
3. If sea ice is absent the oceanic heat loss to the atmosphere yields a strong meridional oceanic temperature gradient which in turn drives the AMOC’s strong circulation mode.
4. In the interstadial configuration the North Atlantic climate system is – although close – not in an equilibrium state. Generally prevailing cold atmospheric temperatures in the high latitudes entail sea ice regrowth, which inevitably drive the system back to the stadial state.
5. The persistence of the interstadial state is highly sensitive to the background conditions.
6. The time-scale separation between ocean, sea ice, and atmosphere (from slow to fast) is central to the characteristic shape of Greenland interstadials in terms of Greenland temperature changes.
7. DO events are stochastically triggered by asymmetric intermittent noise, mimicking abrupt large sea ice removal events.

We hope that our findings will provide a helpful conceptual framework to eventually solve the puzzle of DO variability. The proposed mechanisms should be further tested against new proxy data and by further investigations with Earth system model simulations.

Acknowledgments

This is TiPES contribution #215; the TiPES (‘Tipping Points in the Earth System’) project has received funding from the European Union’s Horizon 2020 research and innovation programme under grant agreement No. 820970. NB acknowledges further funding by the Volkswagen Foundation, the European Union’s Horizon 2020 research and innovation programme under the Marie Skłodowska-Curie grant agreement No. 956170, as well as from the German Federal Ministry of Education and Research under grant No. 01LS2001A.

References

- [1] North Greenland Ice Core Project Members. High-resolution record of Northern Hemisphere climate extending into the last interglacial period. *Nature*, 431: 147–151, 2004. doi: 10.1038/nature02805.
- [2] Dansgaard, W., Clausen, H.B., Gundestrup, N., Hammer, C.U., Johnsen, S.F., Kristinsdottir, P.M., and Reeh, N. A New Greenland Deep Ice Core. *Science*, 218:1273–1277, 1982. doi: 10.1126/science.218.4579.1273.
- [3] Dansgaard, W., Johnsen, S., Clausen, H., Dahl-Jensen, D., Gundestrup, N., Hammer, C., and Oeschger, H. North Atlantic climatic oscillations revealed by deep Greenland ice cores. In *Climate processes and climate sensitivity*, edited by Hansen, J. and Takahashi, T., pages 288–298. American Geophysical Union (AGU), 1984. doi: 10.1029/GM029p0288.
- [4] Johnsen, S.J., Clausen, H.B., Dansgaard, W., Fuhrer, K., Gundestrup, N., Hammer, C.U., Iversen, P., Jouzel, J., Stauffer, B., and Steffensen, J. Irregular glacial interstadials recorded in a new Greenland ice core. *Nature*, 359: 311–313, 1992. doi: 10.1038/359311a0.
- [5] Dansgaard, W., Johnsen, S.J., Clausen, H.B., Dahl-Jensen, D., Gundestrup, N.S., Hammer, C.U., Hvidberg, C.S., Steffensen, J.P., Sveinbjörnsdottir, A.E., Jouzel, J., and Bond, G. Evidence for general instability of past climate from a 250-kyr ice-core record. *Nature*, 364:218–220, 1993. doi: 10.1038/364218a0.
- [6] Jouzel, J., Alley, R.B., Cuffey, K.M., Dansgaard, W., Grootes, P., Hoffmann, G., Johnsen, S.J., Koster, R.D., Peel, D., Shuman, C.A., Stievenard, M., Stuiver, M., and White, J. Validity of the temperature reconstruction from water isotopes in ice cores. *Journal of Geophysical*

- Research: Oceans*, 102:26471–26487, 1997. doi: 10.1029/97JC01283.
- [7] Johnsen, S.J., Dahl-Jensen, D., Gundestrup, N., Steffensen, J.P., Clausen, H.B., Miller, H., Masson-Delmotte, V., Sveinbjörnsdóttir, A.E., and White, J. Oxygen isotope and palaeotemperature records from six Greenland ice-core stations: Camp Century, Dye-3, GRIP, GISP2, Renland and NorthGRIP. *Journal of Quaternary Science*, 16:299–307, 2001. doi: 10.1002/jqs.622.
 - [8] Landais, A., Jouzel, J., Masson-Delmotte, V., and Caillon, N. Large temperature variations over rapid climatic events in Greenland: a method based on air isotopic measurements. *Comptes Rendus - Geoscience*, 337:947–956, 2005. doi: 10.1016/j.crte.2005.04.003.
 - [9] Huber, C., Leuenberger, M., Spahni, R., Flückiger, J., Schwander, J., Stocker, T.F., Johnsen, S., Landais, A., and Jouzel, J. Isotope calibrated Greenland temperature record over Marine Isotope Stage 3 and its relation to CH₄. *Earth and Planetary Science Letters*, 243:504–519, 2006. doi: 10.1016/j.epsl.2006.01.002.
 - [10] Kindler, P., Guillevic, M., Baumgartner, M., Schwander, J., Landais, A., and Leuenberger, M. Temperature reconstruction from 10 to 120 kyr b2k from the NGRIP ice core. *Climate of the Past*, 10:887–902, 2014. doi: 10.5194/cp-10-887-2014.
 - [11] Wolff, E.W., Chappellaz, J., Blunier, T., Rasmussen, S.O., and Svensson, A. Millennial-scale variability during the last glacial: The ice core record. *Quaternary Science Reviews*, 29:2828–2838, 2010. doi: 10.1016/j.quascirev.2009.10.013.
 - [12] Rasmussen, S.O., Bigler, M., Blockley, S.P., Blunier, T., Buchardt, S.L., Clausen, H.B., Cvijanovic, I., Dahl-Jensen, D., Johnsen, S.J., Fischer, H., Gkinis, V., Guillevic, M., Hoek, W.Z., Lowe, J.J., Pedro, J.B., Popp, T., Seierstad, I.K., Steffensen, J.P., Svensson, A.M., Vallelonga, P., Vinther, B.M., Walker, M.J., Wheatley, J.J., and Winstrup, M. A stratigraphic framework for abrupt climatic changes during the Last Glacial period based on three synchronized Greenland ice-core records: Refining and extending the INTIMATE event stratigraphy. *Quaternary Science Reviews*, 106:14–28, 2014. doi: 10.1016/j.quascirev.2014.09.007.
 - [13] Lohmann, J. and Ditlevsen, P.D. Objective extraction and analysis of statistical features of Dansgaard-Oeschger events. *Climate of the Past*, 15:1771–1792, 2019. doi: 10.5194/cp-15-1771-2019.
 - [14] Rial, J.A. and Saha, R. Modeling Abrupt Climate Change as the Interaction Between Sea Ice Extent and Mean Ocean Temperature Under Orbital Insolation Forcing. In *Abrupt Climate Change: Mechanisms, Patterns, and Impacts*, edited by Rashid, H., Polyak, L., and Mosley-Thompson, E., pages 57–74. American Geophysical Union (AGU), 2011. ISBN 9781118670040. doi: 10.1029/2010GM001027.
 - [15] Roberts, A. and Saha, R. Relaxation oscillations in an idealized ocean circulation model. *Climate Dynamics*, 48:2123–2134, 2017. doi: 10.1007/s00382-016-3195-3.
 - [16] Mitsui, T. and Crucifix, M. Influence of external forcings on abrupt millennial-scale climate changes: a statistical modelling study. *Climate Dynamics*, 48:2729–2749, 2017. doi: 10.1007/s00382-016-3235-z.
 - [17] Lohmann, J. and Ditlevsen, P.D. Random and externally controlled occurrences of Dansgaard-Oeschger events. *Climate of the Past*, 14:609–617, 2018. doi: 10.5194/cp-14-609-2018.
 - [18] Boers, N., Ghil, M., and Rousseau, D.D. Ocean circulation, ice shelf, and sea ice interactions explain Dansgaard-Oeschger cycles. *Proceedings of the National Academy of Sciences of the United States of America*, 115:E11005–E11014, 2018. doi: 10.1073/pnas.1802573115.
 - [19] Seierstad, I.K., Abbott, P.M., Bigler, M., Blunier, T., Bourne, A.J., Brook, E., Buchardt, S.L., Buizert, C., Clausen, H.B., Cook, E., Dahl-Jensen, D., Davies, S.M., Guillevic, M., Johnsen, S.J., Pedersen, D.S., Popp, T.J., Rasmussen, S.O., Severinghaus, J.P., Svensson, A., and Vinther, B.M. Consistently dated records from the Greenland GRIP, GISP2 and NGRIP ice cores for the past 104ka reveal regional millennial-scale $\delta^{18}\text{O}$ gradients with possible Heinrich event imprint. *Quaternary Science Reviews*, 106:29–46, 2014. doi: 10.1016/j.quascirev.2014.10.032.
 - [20] Sadatzki, H., Maffezzoli, N., Dokken, T.M., Simon, M.H., Berben, S.M., Fahl, K., Kjær, H.A., Spolaor, A., Stein, R., Vallelonga, P., Vinther, B.M., and Jansen, E. Rapid reductions and millennial-scale variability in Nordic Seas sea ice cover during abrupt glacial climate changes. *Proceedings of the National Academy of Sciences of the United States of America*, 117:29478–29486, 2020. doi: 10.1073/pnas.2005849117.
 - [21] Henry, L.G., McManus, J.F., Curry, W.B., Roberts, N.L., Piotrowski, A.M., and Keigwin, L.D. North Atlantic ocean circulation and abrupt climate change during the last glaciation. *Science*, 353:470–474, 2016. doi: 10.1126/science.aaf5529.
 - [22] Dokken, T.M., Nisancioglu, K.H., Li, C., Battisti, D.S., and Kissel, C. Dansgaard-Oeschger cycles: Interactions between ocean and sea ice intrinsic to the Nordic seas. *Paleoceanography*, 28:491–502, 2013. doi: 10.1002/palo.20042.
 - [23] Berben, S.M., Dokken, T.M., Abbott, P.M., Cook, E., Sadatzki, H., Simon, M.H., and Jansen, E. Independent tephrochronological evidence for rapid and synchronous oceanic and atmospheric temperature rises over the Greenland stadial-interstadial transitions between ca. 32 and 40 ka b2k. *Quaternary Science Reviews*, 236:106277, 2020. doi: 10.1016/j.quascirev.2020.106277.
 - [24] Ezat, M.M., Rasmussen, T.L., and Groeneveld, J. Persistent intermediate water warming during cold stadials

- in the southeastern Nordic seas during the past 65 k.y. *Geology*, 42:663–666, 2014. doi: 10.1130/G35579.1.
- [25] Voelker, A.H. Global distribution of centennial-scale records for Marine Isotope Stage (MIS) 3: A database. *Quaternary Science Reviews*, 21:1185–1212, 2002. doi: 10.1016/S0277-3791(01)00139-1.
- [26] Menviel, L.C., Skinner, L.C., Tarasov, L., and Tzedakis, P.C. An ice–climate oscillatory framework for Dansgaard–Oeschger cycles. *Nature Reviews Earth & Environment*, 1:677–693, 2020. doi: 10.1038/s43017-020-00106-y.
- [27] Ruth, U., Bigler, M., Röthlisberger, R., Siggaard-Andersen, M.L., Kipfstuhl, S., Goto-Azuma, K., Hansson, M.E., Johnsen, S.J., Lu, H., and Steffensen, J.P. Ice core evidence for a very tight link between North Atlantic and east Asian glacial climate. *Geophysical Research Letters*, 34:L03706, 2007. doi: 10.1029/2006GL027876.
- [28] Fischer, H., Siggaard-Andersen, M.L., Ruth, U., Röthlisberger, R., and Wolff, E. Glacial/interglacial changes in mineral dust and sea-salt records in polar ice cores: Sources, transport, and deposition. *Reviews of Geophysics*, 45:RG1002, 2007. doi: 10.1029/2005RG000192.
- [29] Schüpbach, S., Fischer, H., Bigler, M., Erhardt, T., Gfeller, G., Leuenberger, D., Mini, O., Mulvaney, R., Abram, N.J., Fleet, L., Frey, M.M., Thomas, E., Svensson, A., Dahl-Jensen, D., Kettner, E., Kjaer, H., Seierstad, I., Steffensen, J.P., Rasmussen, S.O., Vallelonga, P., Winstrup, M., Wegner, A., Twarloh, B., Wolff, K., Schmidt, K., Goto-Azuma, K., Kuramoto, T., Hirabayashi, M., Uetake, J., Zheng, J., Bourgeois, J., Fisher, D., Zhiheng, D., Xiao, C., Legrand, M., Spolaor, A., Gabrieli, J., Barbante, C., Kang, J.H., Hur, S.D., Hong, S.B., Hwang, H.J., Hong, S., Hansson, M., Iizuka, Y., Oyabu, I., Muscheler, R., Adolphi, F., Maselli, O., McConnell, J., and Wolff, E.W. Greenland records of aerosol source and atmospheric lifetime changes from the Eemian to the Holocene. *Nature Communications*, 9:1476, 2018. doi: 10.1038/s41467-018-03924-3.
- [30] Corrick, E.C., Drysdale, R.N., Hellstrom, J.C., Capron, E., Rasmussen, S.O., Zhang, X., Fleitmann, D., Couchoud, I., Wolff, E., and Monsoon, S.A. Synchronous timing of abrupt climate changes during the last glacial period. *Science*, 369:963–969, 2020.
- [31] Zhang, Y., Chiessi, C.M., Mulitza, S., Sawakuchi, A.O., Häggi, C., Zabel, M., Portilho-Ramos, R.C., Schefuß, E., Crivellari, S., and Wefer, G. Different precipitation patterns across tropical South America during Heinrich and Dansgaard-Oeschger stadials. *Quaternary Science Reviews*, 177:1–9, 2017. doi: 10.1016/j.quascirev.2017.10.012.
- [32] Cheng, H., Sinha, A., Cruz, F.W., Wang, X., Edwards, R.L., D’Horta, F.M., Ribas, C.C., Vuille, M., Stott, L.D., and Auler, A.S. Climate change patterns in Amazonia and biodiversity. *Nature Communications*, 4:1411, 2013. doi: 10.1038/ncomms2415.
- [33] Kanner, L.C., Burns, S.J., Cheng, H., and Edwards, R.L. High-Latitude Forcing of the South American Summer Monsoon During the Last Glacial. *Science*, 335:570–573, 2012. doi: 10.1126/science.1213397.
- [34] Wang, Y.J., Cheng, H., Edwards, R.L., An, Z.S., Wu, J.Y., Shen, C.C., and Dorale, J.A. A high-resolution absolute-dated late pleistocene monsoon record from Hulu Cave, China. *Science*, 294:2345–2348, 2001. doi: 10.1126/science.1064618.
- [35] Broecker, W.S., Peteet, D.M., and Rind, D. Does the ocean-atmosphere system have more than one stable mode of operation? *Nature*, 315:21–26, 1985. doi: 10.1038/315021a0.
- [36] Ganopolski, A. and Rahmstorf, S. Rapid changes of glacial climate simulated in a coupled climate model. *Nature*, 409:153–158, 2001.
- [37] Petersen, S.V., Schrag, D.P., and Clark, P.U. A new mechanism for Dansgaard-Oeschger cycles. *Paleoceanography*, 28:24–30, 2013. doi: 10.1029/2012PA002364.
- [38] Zhang, X., Lohmann, G., Knorr, G., and Purcell, C. Abrupt glacial climate shifts controlled by ice sheet changes. *Nature*, 512:290–294, 2014. doi: 10.1038/nature13592.
- [39] Vettoretti, G. and Peltier, W.R. Fast physics and slow physics in the nonlinear Dansgaard-Oeschger relaxation oscillation. *Journal of Climate*, 31:3423–3449, 2018. doi: 10.1175/JCLI-D-17-0559.1.
- [40] Li, C. and Born, A. Coupled atmosphere-ice-ocean dynamics in Dansgaard-Oeschger events. *Quaternary Science Reviews*, 203:1–20, 2019. doi: 10.1016/j.quascirev.2018.10.031.
- [41] Ganopolski, A. and Rahmstorf, S. Abrupt Glacial Climate Changes due to Stochastic Resonance. *Physical Review Letters*, 88:038501, 2002. doi: 10.1103/PhysRevLett.88.038501.
- [42] Timmermann, A., Gildor, H., Schulz, M., and Tziperman, E. Coherent resonant millennial-scale climate oscillations triggered by massive meltwater pulses. *Journal of Climate*, 16:2569–2585, 2003. doi: 10.1175/1520-0442(2003)016<2569:CRMCOT>2.0.CO;2.
- [43] Menviel, L., Timmermann, A., Friedrich, T., and England, M.H. Hindcasting the continuum of Dansgaard-Oeschger variability: Mechanisms, patterns and timing. *Climate of the Past*, 10:63–77, 2014. doi: 10.5194/cp-10-63-2014.
- [44] Ditlevsen, P.D. Observation of α -stable noise induced millennial climate changes from an ice-core record. *Geophys. Geophysical Research Letters*, 26:1441–1444, 1999.
- [45] Ditlevsen, P.D., Kristensen, M.S., and Andersen, K.K. The recurrence time of Dansgaard-Oeschger events and limits on the possible periodic component. *Journal of Climate*, 18:2594–2603, 2005. doi: 10.1175/JCLI3437.1.

- [46] Ditlevsen, P.D., Andersen, K.K., and Svensson, A. The DO-climate events are probably noise induced: Statistical investigation of the claimed 1470 years cycle. *Climate of the Past*, 3:129–134, 2007. doi: 10.5194/cp-3-129-2007.
- [47] Lohmann, J. and Svensson, A. Ice core evidence for major volcanic eruptions at the onset of Dansgaard-Oeschger warming events. *Climate of the Past Discussions*, 18: 2021–2043, 2022.
- [48] Broecker, W.S., Bond, G., Klas, M., Bonani, G., and Wolfl, W. A salt oscillator in the glacial Atlantic? 1. The concept. *Paleoceanography*, 5:469–477, 1990. doi: 10.1029/PA005i004p00469.
- [49] Rasmussen, T.L. and Thomsen, E. The role of the North Atlantic Drift in the millennial timescale glacial climate fluctuations. *Palaeogeography, Palaeoclimatology, Palaeoecology*, 210:101–116, 2004. doi: 10.1016/j.palaeo.2004.04.005.
- [50] Vettoretti, G., Ditlevsen, P., Jochum, M., and Rasmussen, S.O. Atmospheric CO₂ control of spontaneous millennial-scale ice age climate oscillations. *Nature Geoscience*, 15, 2022. doi: 10.1038/s41561-022-00920-7.
- [51] Gottwald, G.A. A model for Dansgaard-Oeschger events and millennial-scale abrupt climate change without external forcing. *Climate Dynamics*, 56:227–243, 2021. doi: 10.1007/s00382-020-05476-z.
- [52] Hoff, U., Rasmussen, T.L., Stein, R., Ezat, M.M., and Fahl, K. Sea ice and millennial-scale climate variability in the Nordic seas 90 kyr ago to present. *Nature Communications*, 7:12247, 2016. doi: 10.1038/ncomms12247.
- [53] Li, C., Battisti, D.S., and Bitz, C.M. Can North Atlantic Sea Ice Anomalies Account for Dansgaard – Oeschger Climate Signals ? *Journal of Climate*, 23:5457–5475, 2010. doi: 10.1175/2010JCLI3409.1.
- [54] Li, C., Battisti, D.S., Schrag, D.P., and Tziperman, E. Abrupt climate shifts in Greenland due to displacements of the sea ice edge. *Geophysical Research Letters*, 32:1–4, 2005. doi: 10.1029/2005GL023492.
- [55] Lynch-Stieglitz, J. The Atlantic Meridional Overturning Circulation and Abrupt Climate Change. *Annual Review of Marine Science*, 9:83–104, 2017. doi: 10.1146/annurev-marine-010816-060415.
- [56] Stommel, H. Thermohaline Convection with Two Stable Regimes. *Tellus*, 13:224–230, 1961.
- [57] Lisiecki, L.E. and Raymo, M.E. A Pliocene-Pleistocene stack of 57 globally distributed benthic δ 18O records. *Paleoceanography*, 20:1–17, 2005. doi: 10.1029/2004PA001071.
- [58] Eisenman, I. Factors controlling the bifurcation structure of sea ice retreat. *Journal of Geophysical Research Atmospheres*, 117:1–18, 2012. doi: 10.1029/2011JD016164.
- [59] Lohmann, J., Castellana, D., Ditlevsen, P.D., and Dijkstra, H.A. Abrupt climate change as a rate-dependent cascading tipping point. *Earth System Dynamics*, 12: 819–835, 2021. doi: 10.5194/esd-12-819-2021.
- [60] Hasselmann, K. Stochastic climate models: Part I. Theory. *Tellus A: Dynamic Meteorology and Oceanography*, 28:473, 1976. doi: 10.3402/tellusa.v28i6.11316.
- [61] Gottwald, G.A. and Melbourne, I. A Huygens principle for diffusion and anomalous diffusion in spatially extended systems. *Proceedings of the National Academy of Sciences of the United States of America*, 110:8411–8416, 2013. doi: 10.1073/pnas.1217926110.
- [62] Gottwald, G.A. and Melbourne, I. Homogenization for deterministic maps and multiplicative noise. *Proceedings of the Royal Society A*, 469, 2013. doi: https://doi.org/10.1098/rspa.2013.0201.
- [63] Gottwald, G.A., Crommelin, D.T., and Franzke, C.L. Stochastic climate theory. In *Nonlinear and Stochastic Climate Dynamics*, edited by Franzke, C.L.E. and O’Kane, T., pages 209–240. Cambridge University Press, Cambridge, 2017. ISBN 9781316339251. doi: 10.1017/9781316339251.009.
- [64] Fuhrer, K., Neftel, A., Anklin, M., and Maggi, V. Continuous measurements of hydrogen peroxide, formaldehyde, calcium and ammonium concentrations along the new grip ice core from summit, Central Greenland. *Atmospheric Environment Part A, General Topics*, 27:1873–1880, 1993. doi: 10.1016/0960-1686(93)90292-7.
- [65] Kleppin, H., Jochum, M., Otto-Bliesner, B., Shields, C.A., and Yeager, S. Stochastic atmospheric forcing as a cause of Greenland climate transitions. *Journal of Climate*, 28: 7741–7763, 2015. doi: 10.1175/JCLI-D-14-00728.1.
- [66] Drijfhout, S., Gleeson, E., Dijkstra, H.A., and Livina, V. Spontaneous abrupt climate change due to an atmospheric blocking-Sea-Ice-Ocean feedback in an unforced climate model simulation. *Proceedings of the National Academy of Sciences of the United States of America*, 110 :19713–19718, 2013. doi: 10.1073/pnas.1304912110.
- [67] Rasmussen, T.L., Thomsen, E., Van Weering, T.C., and Labeyrie, L. Rapid changes in surface and deep water conditions at the Faeroe Margin during the last 58,000 years. *Paleoceanography*, 11:757–771, 1996. doi: 10.1029/96PA02618.
- [68] Clark, P.U., Dyke, A.S., Shakun, J.D., Carlson, A.E., Clark, J., Wohlfarth, B., Mitrovica, J.X., Hostetler, S.W., and McCabe, A.M. The Last Glacial Maximum. *Science*, 325:710–714, 2009. doi: 10.1126/science.1172873.
- [69] Sadatzki, H., Dokken, T.M., Berben, S.M., Muschiatiello, F., Stein, R., Fahl, K., Menviel, L., Timmermann, A., and Jansen, E. Sea ice variability in the southern norwegian sea during glacial dansgaard-oeschger climate cycles. *Science Advances*, 5:1–11, 2019. doi: 10.1126/sciadv.aau6174.

- [70] Gottschalk, J., Skinner, L.C., Misra, S., Waelbroeck, C., Menviel, L., and Timmermann, A. Abrupt changes in the southern extent of North Atlantic Deep Water during Dansgaard-Oeschger events. *Nature Geoscience*, 8:950–954, 2015. doi: 10.1038/ngeo2558.
- [71] Rasmussen, T.L., Thomsen, E., Labeyrie, L., and Van Weering, T.C. Circulation changes in the Faeroe-Shetland Channel correlating with cold events during the last glacial period (58-10 ka). *Geology*, 24:937–940, 1996. doi: 10.1130/0091-7613(1996)024<0937:CCITFS>2.3.CO;2.
- [72] Klockmann, M., Mikolajewicz, U., Kleppin, H., and Marotzke, J. Coupling of the Subpolar Gyre and the Overturning Circulation During Abrupt Glacial Climate Transitions. *Geophysical Research Letters*, 47, 2020. doi: 10.1029/2020GL090361.
- [73] Jensen, M.F., Nilsson, J., and Nisancioglu, K.H. The interaction between sea ice and salinity-dominated ocean circulation: implications for halocline stability and rapid changes of sea ice cover. *Climate Dynamics*, 47:3301–3317, 2016. doi: 10.1007/s00382-016-3027-5.
- [74] Singh, H.A., Battisti, D.S., and Bitz, C.M. A heuristic model of dansgaard-oeschger cycles. part i: Description, results, and sensitivity studies. *Journal of Climate*, 27: 4337–4358, 2014. doi: 10.1175/JCLI-D-12-00672.1.

Supporting information for

Glacial abrupt climate change as a multi-scale phenomenon resulting from monostable excitable dynamics

Keno Riechers, Georg Gottwald & Niklas Boers (2023) [arXiv preprint]

Corresponding Author: Keno Riechers, riechers@pik-potsdam.de

Ocean component We adopt the classical Stommel model [1] for the dynamics of the oceanic meridional gradients of temperature $T = T_e - T_p$ and salinity $S = S_e - S_p$, where the subscripts denote the respective equatorial and northern polar variables [2, 3]

$$\tau_{\text{ocean}} \dot{T} = -\gamma(I)(T - \theta) - (1 + \mu |T - S|)T, \quad (1)$$

$$\tau_{\text{ocean}} \dot{S} = \sigma - (1 + \mu |T - S|)S. \quad (2)$$

In Eq. 2 σ denotes a freshwater forcing that sustains a meridional salinity gradient. The term $(1 + \mu |T - S|)$ represents diffusive and advective transport of heat and salt within the ocean, both counteracting existing meridional gradients. The flux parameter μ is a measure for the relative strength of the advective transport with respect to the diffusive transport. The flow $q = T - S$ quantifies the strength of the AMOC, which is driven by a meridional density gradient resulting from temperature and salinity differences between the equatorial and polar boxes. The term $\gamma(I)(T - \theta)$ describes the relaxation of the oceanic temperatures to the prevailing atmospheric temperatures θ . The key modifications that we apply to the Stommel model are related to this term. First, in the original Stommel model the atmospheric temperature gradient θ is a constant and describes a static climatic background. Given that the relaxation of oceanic temperatures T to atmospheric temperatures θ requires mutual exchange of heat between atmosphere and ocean, we argue that the heat transfer should impact the atmospheric temperature gradient as well. We therefore treat θ as an additional dynamic variable as described in the next section. Second, we model the rate of the atmosphere–ocean heat exchange γ , which is also a constant in the original Stommel model, as a function of the Nordic Seas’ sea ice cover I . The latter acts as an insulator between the two media. With sea ice being the fourth dynamical variable of our model, the rate $\gamma(I)$ is subject to dynamic changes. This mechanism will be described in detail further below.

Atmosphere component We explicitly take into account the effect of the atmosphere–ocean heat exchange on the atmospheric meridional temperature gradient by writing

$$\dot{\theta} = -\Gamma(\theta - \theta_0) - \gamma(\theta - T)/\kappa. \quad (3)$$

Here, θ_0 is the atmospheric temperature gradient determined by the background climate state, which would dictate $\theta(t)$ in the absence of the ocean–atmosphere feedback. The relaxation of $\theta(t)$ towards θ_0 at the rate Γ competes with the relaxation of the atmosphere towards the oceanic temperature gradient T which acts at a rate γ/κ . The introduction of an atmospheric heat capacity κ guarantees that the heat flux between ocean and atmosphere is consistently incorporated in the equations of motion of θ and T in compliance with energy conservation. In the limit of infinitely fast relaxation of the atmospheric temperature gradient θ against the background climate θ_0 , the original Stommel model with constant $\theta = \theta_0$ is recovered. Multiplication of Eq. 3 by κ yields the atmosphere dynamics

$$\tau_{\text{atm}} \dot{\theta} = -\eta(\theta - \theta_0) - \gamma(I)(\theta - T) \quad (4)$$

with $\tau_{\text{atm}} = \kappa$; in this case $\eta = \kappa\Gamma$ represents an effective atmospheric heat dissipation rate. The heat capacity of the atmosphere thus introduces a time scale separation between the oceanic and atmospheric components of our model. In the following we call the ocean–atmosphere system defined by Eqs. 1–4 with a constant relaxation rate γ and without the stochastic forcing ζ_t used in the main text the extended Stommel model.

Dynamics of the extended Stommel model We now discuss the dynamics of the extended Stommel model defined by Eqs. 1–4 for constant relaxation rate γ and constant background state θ_0 . Figure 1 shows the model’s bifurcation diagram with γ acting as a bifurcation parameter. As the standard Stommel model, the extended model has two stable fixed point branches. For $1.1 < \gamma < 1.21$ the system is bistable with an unstable branch separating the two stable ones. The lower branch is associated with a weak mode of overturning (smaller $|q|$) while the upper branch represents a strong mode (larger $|q|$), with the former being salinity-driven ($S > T$) and the latter being temperature-driven ($T > S$). We note that the increase of q with increasing γ is stronger in the standard Stommel model because in the extended model a strengthening of the AMOC weakens the atmospheric temperature gradient.

Given the interpretation of the model variables established in the main text, with θ corresponding to arctic atmospheric temperatures, T representing the Nordic Seas’ deep and intermediate water temperatures and q indicating the AMOC strength, we can identify stadial and interstadial climate conditions with different configurations of the extended Stommel model. The ocean–atmosphere heat exchange rate γ controls the state of the high latitude climate (Fig. 1). Varying γ from low to high

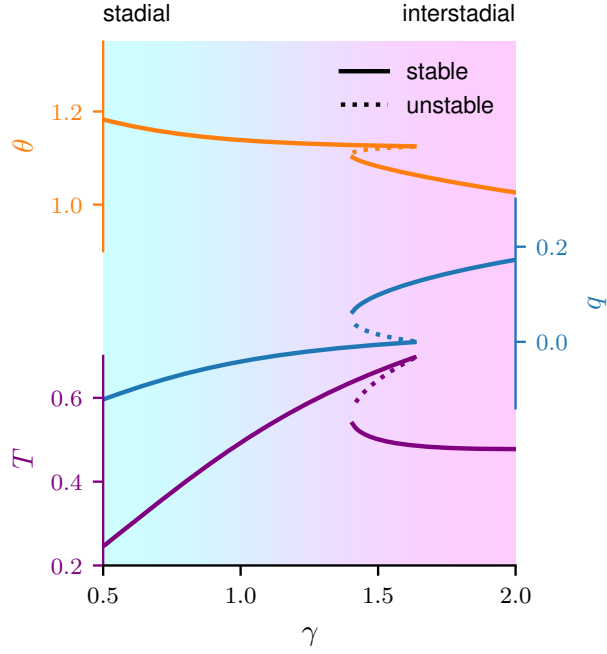


Figure 1: Bifurcation diagram of the extended Stommel model defined by Eqs. 1-4. The heat exchange rate γ acts as a control parameter with two bifurcations occurring at $\gamma_{c1} = 1.1$ and $\gamma_{c2} = 1.21$. Solid (dashed) lines represent stable (unstable) branches. The atmospheric meridional temperature gradient θ declines with increasing heat exchange rate γ due to the action of the ocean on the atmosphere. The stable branch of the model that is associated with higher γ is commonly referred to as the strong mode (temperature driven), while the stable branch associated with lower γ is called the weak mode (salinity driven). For low $\gamma < 0.8$ all model variables assume a stadial configuration (blue shading), while for $\gamma > 1.5$ they assume an interstadial configuration (magenta shading). Here, the atmospheric background climate was set to $\theta_0 = 1.3$ and all other parameters are as given in the main text.

values yields changes in all three model variables that consistently match the changes of the true climate system observed between stadial and interstadial periods. Low values of $\gamma \lesssim 0.7$ are associated with a weak AMOC state (lower $|q|$ as compare to the strong stable AMOC branch), cold polar atmosphere (large θ) and warm Nordic Seas (small T), while high values of $\gamma \gtrsim 1.5$ reverse this configuration. This allows to interpret the stable states of the extended Stommel model at low and high γ as stadial and interstadial states, respectively.

Although higher values of γ entail enhanced oceanic northward heat transport, the Nordic Seas are colder in this configuration because of the stronger release of heat into the atmosphere. In the stadial state (small values of γ) the model shows sustained northward heat transport provided by the salinity-driven weak AMOC. However, with the corresponding smaller heat exchange rate γ even a reduced northward heat transport warms the northern ocean as it hardly loses any heat to the atmosphere. This model behavior is in line with the findings by [4–6] who report a sustained warm water inflow into the Nordic seas at intermediate depth during stadials.

Sea ice component The sea ice variable I represents the sea ice cover in the polar box (i.e. in the Nordic Seas). Acting as an insulator, the sea ice controls the heat exchange rate γ between the polar atmosphere and ocean [5, 7]. We adopt the seasonally averaged version of the [8] sea ice model introduced by [9]:

$$\dot{I} = \Delta \tanh\left(\frac{I}{h}\right) - R_0 \Theta(I) I + L - B I, \quad (5)$$

where $\Theta(I)$ denotes the Heaviside function. The first term represents the ice-albedo feedback to the incoming solar short-wave radiation. The sea ice transport, which is absent in open ocean conditions ($I < 0$), is controlled by R_0 . The term $L - BI$ describes the change of sea ice due to the net outgoing longwave radiation (OLR) according to a linearized Stefan Boltzmann law. The incoming longwave radiation depends on the atmospheric temperature θ . In order to incorporate dynamic changes of the polar atmospheric temperature in Eq. 5 and to couple the sea ice model with the extended Stommel model, we assume a linear relationship between the net incoming (or outgoing) longwave radiation and the atmospheric temperature and write

$$L = L_0 + L_1(\theta - \theta^*), \quad (6)$$

where $\theta - \theta^*$ denotes deviations from some default atmospheric temperature. Since larger θ corresponds to a colder polar atmosphere with positive effect on the sea ice growth, L_1 is positive. Inserting Eq. 6 into Eq. 5 finally leads to our sea ice model used in the main text

$$\tau_{ice} \dot{I} = \Delta \tanh\left(\frac{I}{h}\right) - R_0 \Theta(I) I - L_0 + L_1 \theta - L_2 I + \xi_t, \quad (7)$$

yet without the stochastic forcing ξ_t . We ignore influences of the oceanic temperatures on the sea ice.

In the original Eisenman model I is the negative of the enthalpy which is proportional to the thickness of the sea ice if $I > 0$. [8] considered an oceanic box of limited size, such that the sea ice can be regarded as homogeneous along the horizontal dimensions of the box. In our case, the polar oceanic box is identified with the Nordic Seas and is thus too large for such a homogeneity assumption to hold and therefore the variable I in our model should be interpreted as a measure of the annually averaged sea ice volume in the Nordic Seas (and the northern North Atlantic) with $I = 0$ indicating intermediate sea ice cover.

As mentioned previously, sea ice insulates atmosphere and ocean from one another and hence controls their mutual heat exchange. Note that the heat flux ψ between any two reservoirs with different temperatures is proportional to their temperature difference ΔT . If separated by an insulator, ψ is moreover inversely proportional to the insulator's thickness. Based on our altered interpretation of the sea ice variable I , we model the effect of the sea ice on the ocean–atmosphere heat exchange in form of a hyperbolic tangent with saturation towards high and low values of sea ice

$$\gamma(I) = \gamma_0 + \frac{\Delta\gamma}{2} \left[\tanh\left(\frac{-(I - I_0)}{\omega}\right) + 1 \right]. \quad (8)$$

This yields a heat flux $\psi \propto \gamma(I) (T - \theta)$ that in turn controls the mutual atmosphere–ocean relaxation in terms of temperatures. The parameters γ_0 and $\gamma_0 + \Delta\gamma$ in Eq. 8 define the heat exchange rate at maximum ice cover and open ocean conditions, respectively, and ω moderates the steepness of the heat exchange decline with increasing sea ice thickness I . Shifting the hyperbolic tangent along the sea ice axis by setting $I_0 = -0.5$ yields an already substantially reduced heat exchange rate at intermediate sea ice cover ($I = 0$; cf. Fig. 2). At maximum sea ice cover the heat exchange between the high-latitude ocean and atmosphere is considered to be (almost) shut off. At low latitudes, the heat flux is unaffected by the sea ice and thus the total ocean–atmosphere heat flux is sustained at the reduced rate γ_0 even with fully sea ice covered Nordic Seas. We assume that the atmosphere–ocean temperature difference is larger in the polar box than in the equatorial box, with the effect that polar heat exchange contributes stronger to the relaxation of the gradients θ and T to one another. This justifies a relatively small minimum exchange rate $\gamma_0 = 0.5$ compared to the maximum heat exchange rate $\gamma_0 + \Delta\gamma = 4$.

We now examine the joint bifurcation structure of the sea ice model and the atmospheric temperature θ in the deterministic setting — i.e. we assess the nullclines of Eqs. 4 and 7. Our sea ice model features a double fold bifurcation with respect

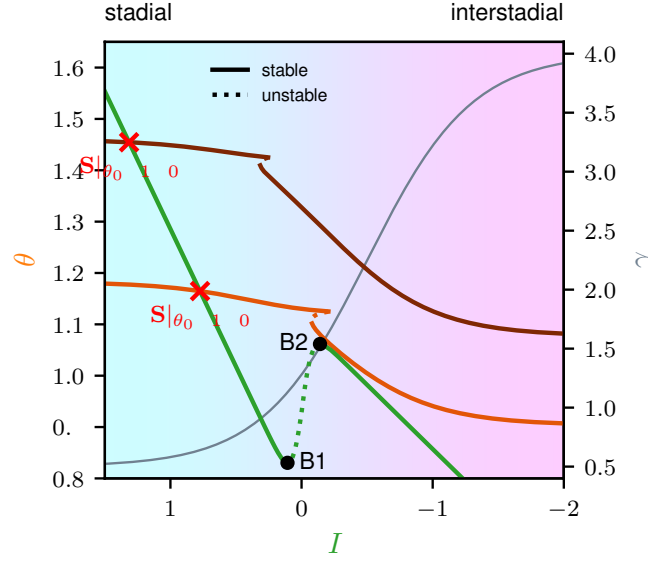


Figure 2: Nullcline of the seasonally averaged sea ice I (green) together with the nullcline of the Stommel atmosphere θ (orange). Due to the ice-albedo feedback the sea ice model features a bistable region where an ice-rich and a low-ice solution coexist. The difference in the slope of the two stable branches is controlled by the strength of the sea ice export R_0 . The upper θ -nullcline (dark orange) is the same as in Fig. 1 with $\theta_0 = 1.45$ upon using the transformation $\gamma = \gamma(I)$ given by Eq. 8. The lower θ -nullcline (lighter orange) results from setting $\theta_0 = 1.3$. The heat exchange rate $\gamma(I)$ as a function of the sea ice is shown in light gray on the right ordinate. Intersections of the θ and I nullclines define fixed points of the entire coupled system defined by Eqs. 1–8. Larger atmospheric backgrounds θ_0 yield more pronounced stadial conditions with colder arctic atmosphere and larger sea ice cover.

to θ (Fig. 2). The associated bistability is an effect of the ice–albedo feedback. The bifurcation points are given by $B1 = (\theta = 0.83, I = 0.11)$ and $B2 = (\theta = 1.06, I = -0.14)$. Intersections of the sea ice’s and the atmosphere’s nullclines constitute fixed points of the full coupled system. The stable fixed points that correspond to the two climate background states $\theta_0 = 1.3$ and $\theta_0 = 1.45$ are $(\theta_s \sim 1.16, I_s \sim 0.77)$ and $(\theta_s \sim 1.31, I_s \sim 1.05)$, respectively, and represent stadial climate states with large sea ice cover and cold temperatures over Greenland (crosses in Figure 2). Note that larger atmospheric background gradients yield a more severe stadial climate with larger I_s and θ_s . The corresponding stadial fixed point in the ocean model, i.e. in Eqs. 1 and 2 is $T_s \approx 0.3$ for both values of θ_0 , implying relatively warm Nordic Seas. Moreover, the AMOC strength $q_s \sim -0.09$ is negative and thus salinity driven and weak.

A key feature of the bifurcation diagram is the proximity of the low-ice stable branch of the sea ice nullcline and the strong-mode stable branch of the θ nullcline around $I \approx -0.25$. The closer the nullclines are to each other, the slower is the deterministic dynamics in nearby regions of the state space. Their distance is controlled by the atmospheric climate background θ_0 and decreases with decreasing θ_0 provided that $\theta_0 > 1.29$. If the nullclines are sufficiently close, once the system enters this region of the state space, the dynamics allows for prolonged periods in which I and θ do not vary much, giving rise to what we term a meta-stable state. It is the existence of this transient meta-stable state that allows us to model interstadials.

To bring the system close to the meta-stable state we require sufficiently large perturbations. In our model these will be provided by substantial stochastic sea ice removals which reactivate the ocean–atmosphere interaction and thereby trigger temporary state space excursions into the interstadial regime. This is achieved by introducing a non-Gaussian intermittent stochastic process which acts as a forcing on the sea ice and is capable of inducing the required large abrupt sea ice removal.

References

- [1] Stommel, H. Thermohaline Convection with Two Stable Regimes of Flow. *Tellus*, 13:224–230, 1961. doi: 10.1111/j.2153-3490.1961.tb00079.x.
- [2] Cessi, P. A Simple Box Model of Stochastically Forced Thermohaline Flow. *Journal of Physical Oceanography*, 24: 1911–1920, 1994. doi: [https://doi.org/10.1175/1520-0485\(1994\)024<1911:ASBMOS>2.0.CO;2](https://doi.org/10.1175/1520-0485(1994)024<1911:ASBMOS>2.0.CO;2).
- [3] Roeber, P.J. Climate variability in a low-order coupled atmosphere–ocean model. *Tellus A*, 47:473–494, 1995. doi: 10.1034/j.1600-0870.1995.t01-3-00006.x.

- [4] Rasmussen, T.L. and Thomsen, E. The role of the North Atlantic Drift in the millennial timescale glacial climate fluctuations. *Palaeogeography, Palaeoclimatology, Palaeoecology*, 210:101–116, 2004. doi: 10.1016/j.palaeo.2004.04.005.
- [5] Dokken, T.M., Nisancioglu, K.H., Li, C., Battisti, D.S., and Kissel, C. Dansgaard-Oeschger cycles: Interactions between ocean and sea ice intrinsic to the Nordic seas. *Paleoceanography*, 28:491–502, 2013. doi: 10.1002/palo.20042.
- [6] Ezat, M.M., Rasmussen, T.L., and Groeneveld, J. Persistent intermediate water warming during cold stadials in the southeastern Nordic seas during the past 65 k.y. *Geology*, 42:663–666, 2014. doi: 10.1130/G35579.1.
- [7] Boers, N., Ghil, M., and Rousseau, D.D. Ocean circulation, ice shelf, and sea ice interactions explain Dansgaard-Oeschger cycles. *Proceedings of the National Academy of Sciences of the United States of America*, 115:E11005–E11014, 2018. doi: 10.1073/pnas.1802573115.
- [8] Eisenman, I. Factors controlling the bifurcation structure of sea ice retreat. *Journal of Geophysical Research Atmospheres*, 117:D01111, 2012. doi: 10.1029/2011JD016164.
- [9] Lohmann, J., Castellana, D., Ditlevsen, P.D., and Dijkstra, H.A. Abrupt climate change as a rate-dependent cascading tipping point. *Earth System Dynamics*, 12:819–835, 2021. doi: 10.5194/esd-12-819-2021.